
Radiometric calibration of ocean color remote sensing instruments

Fall 2017

Sivert Bakken

Supervisors: Harald Martens, Tor Arne Johansen, João Fortuna
NTNU - ITK



Norwegian University of
Science and Technology



Overview

This project should investigate different approaches to perform radiometric calibration for ocean color remote sensing satellite instruments. That is, how to improve the quality and validity of remotely sensed earth observations, focused on the field of ocean color observations.

Goals

1. Understand the concept of hyperspectral imaging, how it is captured, its limitations.
2. Get familiar with the “Data Processing Levels” (from NASA, ESA).
3. Investigate different approaches for radiometric calibration for remote sensing satellite instruments.
4. Investigate current and prior ocean color remote sensing systems
5. Simulate and analyze different error dynamics for ocean color remote sensing instruments.

Specifications

Preface

I would like to thank my supervisors: Harald Martens, Tor Arne Johansen, and João Fortuna , for letting me solve this task so freely.

As I was not familiar with the topic of remote sensing, oceanography, hyperspectral or multispectral imaging or ocean color before working on this project thesis, the freedom provided has been appreciated. Through familiarizing myself with the aforementioned topics I have learned a lot, and it has piqued my interest within fields not strongly related to my academic background, in a way broadening my horizon.

For most of the images within this document, their reuse has not been communicated to the original owner of the image. All of the images should have a reference as to where to find the original source of the image. It is important to note that this document is not supposed to be sold or distributed, as this may result in legal issues. It is only intended for internal use.

Abstract

In this project thesis, the different approaches to performing radiometric calibration of ocean color remote sensing satellites, especially considering the NTNU SmallSat Program, have been investigated. The documents consist of a brief introduction to ocean remote sensing, followed by a description of definitions and challenges regarding radiometric calibration and potential approaches to alleviate these challenges. A simulation displaying some of the potential distortions is provided as well. Lastly, there is a short discussion of the findings and the road ahead.

Acronyms

AVIRIS Airborne Visible / Infrared Imaging Spectrometer.

BRDF Bidirectional reflectance distribution function.

CDOM Colored Dissolved Organic Matter.

CEOS Committee on Earth Observation Satellite.

ESA European Space Agency.

HICO Hyperspectral Imager for Coastal Ocean.

IOCCG International Ocean Color Coordinating Group.

ISS International Space Station.

MERIS MEdium Resolution Imaging Spectromete.

MOBY Marine Optical Buo.

MODIS Moderate Resolution Imaging Spectroradiometer.

NASA National Aeronautics and Space Administration (US).

NIR Reffering to the spectral bands in the near-infrared.

Pixel Abbreviation of pixel element.

SeaWiFS Sea-viewing Wide Field-of-view Senso.

SRCA Spectroradiometric Calibration Assembly.

SWIR Reffering to the spectral bands in the short-wave infrared.

TOA Top of atmosphere.

VIIRS Visible Infrared Imaging Radiometer Suit.

VISNIR Referring to the spectral bands in the visual to near-infrared.

Glossary

F_0 Extraterrestrial solar irradiance.

f_b Bidirectional reflectance correction.

f_b^t Targeted bidirectional reflectance correction.

f_λ Band-pass adjustment to L_{wn} .

f_λ^t Band-pass adjustment to L_{wn}^t .

f_p Polarization correction factor.

f_s EarthSun distance correction.

f_s^t Targeted EarthSun distance correction.

\bar{g} Mean vicarious gain.

g_i Vicarious gain for calibration sample at date and location i.

L_a Radiance due to scatter by aerosol and Rayleigh-aerosol interactions.

λ Wavelength, often referring to wavelength at sensor.

L_f Radiance associated with foam on the sea surface.

L_r Radiance due to Rayleigh scattering from air molecules.

L_t Observed top of the atmosphere radiance.

L_t^t Targeted top of the atmosphere radiance.

L_w Retrieved water leaving radiance..

L_w^t Targeted water leaving radiance.

μ_s Cosine of solar zenith angle.

μ_s^t Targeted cosine of solar zenith angle.

θ_0 Solar zenith angle.

t_{d_s} Rayleigh-aerosol diffuse transmittance for solar path.

$t_{d_s}^t$ Targeted rayleigh-aerosol diffuse transmittance for solar path.

$t_{d_v}^t$ Rayleigh-aerosol diffuse transmittance for view path.

t_{g_s} Transmittance due to gaseous absorption for solar path.

$t_{g_s}^t$ Targeted transmittance due to gaseous absorption for solar path.

t_{g_v} Transmittance due to gaseous absorption for sensor view path.

θ_s Zenith angle for solar path.

θ_v Zenith angle for view path.

Table of Contents

Preface	3
Preface	3
Acronyms	5
Glossary	7
Table of Contents	10
1 Introduction	11
2 Background Theory	13
2.1 Hyperspectral imaging and processing	13
2.1.1 Hyperspectral Image Acquisition	15
2.2 Ocean surface and Electromagnetic Radiation	16
2.2.1 Ocean Surface	16
2.2.2 Electromagnetic radiation	17
2.3 Ocean Remote Sensing From Satellites	19
2.3.1 Orbits for ocean remote sensing	20
2.3.2 Image acquisition for ocean remote sensing	20
2.3.3 Processing levels and archives	21
2.4 Atmosphere and Atmospheric Correction	22
2.5 Ocean Color	25
2.6 International Efforts for Earth Observations	26
3 In-flight Calibration and inter-calibration of Satellite instruments	27
3.1 Calibration & Validation	27
3.1.1 Definitions and Requirements	27
3.1.2 General Calibration Problems	29
3.2 On-board calibration techniques	30

3.2.1	Lamp Calibration	30
3.2.2	Lunar Calibration	30
3.2.3	Solar Calibration	31
3.3	Calibration Using Naturally Occurring Phenomena	32
3.3.1	Pseudo-Invariant Calibration Sites	32
3.3.2	Deep Convective Clouds	32
3.3.3	Rayleigh Scattering	33
3.3.4	Sun Glint	34
3.4	System Absolute Calibration	35
3.4.1	Other approaches	37
4	Experiences From Historical and Current Ocean Remote Sensing Systems	39
4.1	Hyperspectral Imager for Coastal Oceans	40
4.1.1	Mission and instrument	40
4.1.2	Problems and Vicarious Calibration	40
4.1.3	Heritage	41
4.2	Medium Resolution Imaging Spectrometer	41
4.2.1	Mission and instrument	41
4.2.2	Calibration	42
4.3	Sea-viewing Wide Field-of-view Sensor	42
4.3.1	Mission and instrument	42
4.3.2	Calibration	42
4.3.3	Heritage	43
4.4	Moderate-resolution Imaging Spectroradiometer	44
4.4.1	Mission and instrument	44
4.4.2	Calibration	44
4.5	The Pre-Aerosol, Clouds and ocean Ecosystem	46
5	Simulation	47
5.1	Methodology and Implementation	47
5.2	Simulation results	49
6	Discussion & Conclusion	53
6.1	Future work and recommendations	54
6.1.1	Camera characterization	54
6.1.2	Hyperspectral Ocean Color Remote Sensing	55
Bibliography		55
Appendices		63
A Correspondence		65
B How to perform simulation		71

Introduction

The ocean is intertwined with all life on Earth. Approximately 70% of the Earth's surface consists of water, and 25% of the total planetary vegetation resides in the ocean [1]. To be able to understand the dynamics of the world it is paramount to understand the dynamics of the ocean. The data gathered from oceanographic observations are used for weather and storm predictions, monitoring of aquaculture and biological sea life, monitoring of long-term sea temperature changes and much much more. Since the launch of the first satellite proof-of-concept instrument predominantly designed for remote sensing of water, the Coastal Zone Color Scanner or CZCS aboard Nimbus 7 [2] in 1978, the technology has grown rapidly. Today, almost four decades later, there are eight data generating ocean color remote sensing instruments operative[3], and since 1978 23 such satellites have retired.

The Norwegian continental shelf is four times the area of the Norwegian mainland and constitutes about one-third of the European continental shelf, and with it, Norway becomes the second largest country in Europe [4]. Thus it is safe to say that the ocean is of particular importance to Norwegian society and economy. In an effort to meet this demands in Norwegian society and industry, the Norwegian University of Science and Technology (NTNU), is currently developing a small satellite program for multi-agent marine observations [5], hereafter named the NTNU SmallSat Program. The NTNU SmallSat Program will be equipped with a Hyperspectral image sensor suitable for (other) autonomous vehicles as well e.g. UAVs. This program will hopefully be the beginning of a dedicated constellation of ocean observing satellites, designated to the Norwegian coast, and cooperating with other autonomous ocean observing systems.

This project thesis is created in an effort to enlighten some of the procedures necessary to create data records of any value to scientists when conducting remote sensing of the Earth and specifically of ocean color, mainly focusing on the difficulties of radiometric calibration.

The 2nd chapter will provide the reader with the sufficient background material regarding ocean color remote sensing and hyperspectral imaging, or refer the reader to good sources regarding the topic. The 3rd chapter will investigate different approaches to perform radiometric calibration and discuss their strengths, weaknesses, and requirements. The 4th chapter will look at existing and prior ocean color remote sensing systems. The 5th chapter will investigate how different types of errors in remotely sensed data may behave. Lastly, the 6th chapter will discuss the findings and relate them to the NTNU SmallSat Program.

Chapter 2

Background Theory

2.1 Hyperspectral imaging and processing

This section is mainly developed from the book *Hyperspectral Imaging Technology in Food and Agriculture* by B. Park and R. Lu [6].

Hyperspectral Image processing is the collective term for using different types of algorithms to derive, manipulate or store information from relevant spectral bands[6]. A hyperspectral image collects and processes information from across the electromagnetic spectrum with an objective to obtain the spectrum for each pixel in the image of a scene for analysis e.g. identifying materials or detecting processes. The spectral bands most often associated with hyperspectral image processing lies within the domain of visible to near-infrared light, often shortened down to VNIR or VISNIR. The algorithms used in hyperspectral imaging handle such problems as classification and detection, all with a goal of better understanding the image or the object in the image. Hyperspectral image processing is in general concerned with the wavelengths between 400-1,700 nm as shown in figure 2.2. There are limitations to the measurements that Hyperspectral sensors may bring and figure 2.1 displays to some extent the uncertainties that hyperspectral imaging will bring as a result of illumination and reflectance angle differences.

Remote sensing for oceanographic observation from space, which is the objective of the NTNU SmallSat program, has been mainly concerned with multispectral instruments [1]. Thus it should be noted that the exercise of hyperspectral image processing borrows a lot of its techniques from other fields. Fields such as chemometrics and spectroscopy, but also machine learning and data analytics, compared to more traditional ocean remote sensing. These fields can contribute to some unique insights that traditional remote sensing techniques do not provide when handling hyperspectral data. [7, 6]. As Remote sensing traditionally only use a few spectral bands as a part of its analysis a lot of information and insight of the scene will be lost to the low spectral resolution. However, as the spectral resolution increases the importance of high spatial resolution increases as well. It's not trivial to distinguish between the spectral responses of different objects. If the spec-

tral response of several objects is captured in one pixel, distinguishing between them will be even more complicated. An image consisting of a hyperspectral data can inherently be considered a multidimensional or multivariate problem. Techniques such as PCA and PLSR can be used to process the spectral information and to gain insights. These methods are well-established approaches within the fields of chemometrics, food analytics and precision agriculture [8].

Depending on which source you rely on one can say that the hyperspectral domain starts once you surpass 30 spectral bands, but typically contains 100 bands [9, 6, 10], and with relatively high spectral resolution when compared to other multispectral instruments.

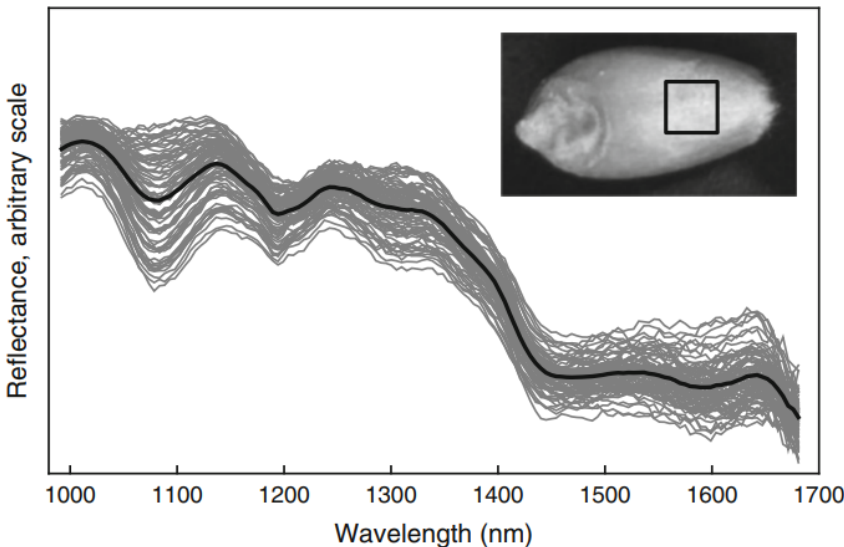


Figure 2.1: the spectra of 9x9 pixels of a wheat kernel. This practical example shows that it is not trivial to determine what kind of object the spectral response originates from. The black line is the average intensity of all the pixels. Image courtesy of Park & Lu [6].

The workflow of hyperspectral image processing is quite different than the workflow often associated with traditional RGB/BW-image processing. The pipeline is shown in figure 2.3. The workflow is complicated as it is inherently a multidisciplinary and demands in-depth knowledge from fields such as camera optics, Electronics, Software and specific domain knowledge of the object being captured. The subject of this text is marked in red of figure 2.3, and when the application of the hyperspectral image processing is Remote sensing, the act of atmospheric correction falls within the calibration block in the general workflow pipeline.

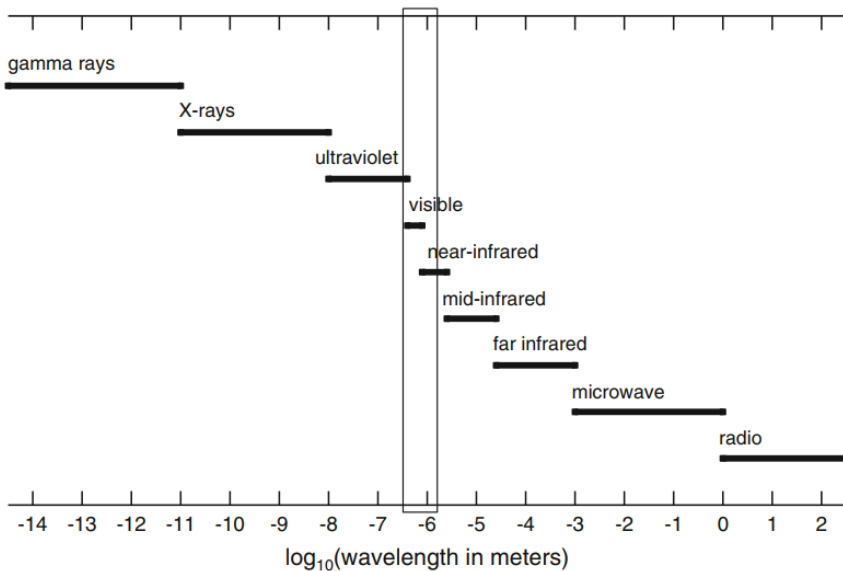


Figure 2.2: An Illustration of the spectra most commonly used in hyperspectral imaging, accompanied with other electromagnetic named bands. Image courtesy of Park & Lu [6].

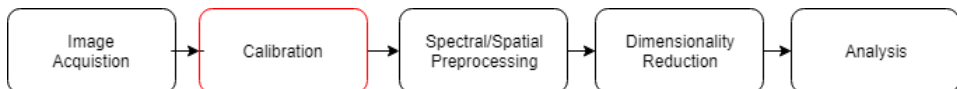


Figure 2.3: General workflow pipeline for Hyperspectral image processing as described by Park & Lu[6].

2.1.1 Hyperspectral Image Acquisition

There are two distinct system types for capturing hyperspectral images [6], namely the pushbroom line scanner and the area scanner. The area scan system for acquiring hyperspectral images works by placing a variable electronic filter in front of a two-dimensional monochromatic camera i.e. a camera that only captures at specific wavelengths at, changed by the filter. The filter then adjusts to determine which wavelength to be currently captured[6]. This method is not preferred in moving systems. A more appropriate method for systems in motion is a pushbroom line scanning system. The system will capture a line in the cross-track direction for all spectral bands at a time. The motion of the entire system will provide the along-track image acquisition, through translation, attitude change or a combination of the two. An illustration of the process is provided in figure 2.4. This approach is popular and widespread in airborne systems[11, 6].

In recent years it has been feasible to develop systems with hyperspectral instruments for Remote sensing satellites, and the NTNU SmallSat Program will have a hyperspectral camera as payload[5].

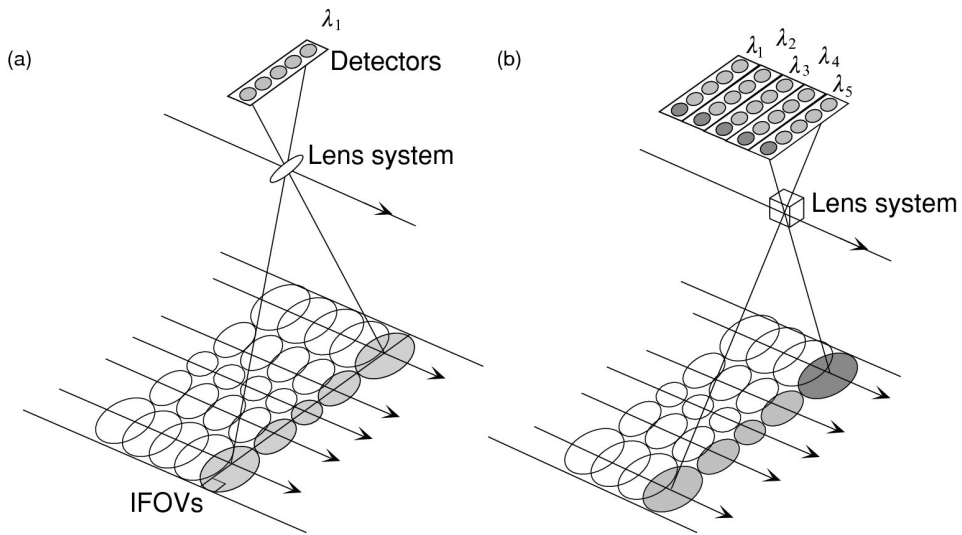


Figure 2.4: An Illustration of the operating modes of a push-broom scanner. The arrows indicating the direction of the system, and the grey circles the line of interest. The Image courtesy of S. Martin[1].

2.2 Ocean surface and Electromagnetic Radiation

What one will be able to observe from an ocean remote sensing satellite is determined by ocean surface properties, the object to be imaged, and properties determined by the physics of electromagnetic radiation transmitted and the path it has taken. The two subsequent subsection will follow the descriptions of S. Martin [1].

2.2.1 Ocean Surface

For Ocean remote sensing it is important to understand ocean surface phenomena. There are certain open ocean properties that affect the emitted and reflected radiation at all frequencies. Some phenomena worth noting can be listed as follows:

1. Wind-generated capillary waves and gravity waves
2. Breaking waves and the generation and decay of foam
3. The modulation of short waves and currents by large waves and currents.
4. Natural and human-made slicks

The first element of the list above, capillary waves, perhaps better known as ripples, is a type of wave traveling along the phase boundary of the medium and whose dynamics and phase velocity is dominated by surface tension effects. These capillary effects are mainly important for centimeter-scale events, but at large scales, this will directly affect what is possible to see from a remote sensing satellite. The gravity-induced waves are created due to the force of gravity and buoyancy trying to reach an equilibrium. These waves

will change the wave profile dependent on their amplitude. Ocean surface waves can be described by the following equation:

$$\eta = a_w \sin(k_w x - \omega_w t) \quad (2.1)$$

Where a_w is the amplitude, the wave number given by k_w and the radian frequency given by $\omega_w = 2\pi/T_w$. A small amplitude, i.e. $a_w k_w \ll 1$ indicates that the wave is mainly affected by gravity effects and has a nice sinusoidal form. As $a_w k_w$ rises the waveform will have additions of higher-order harmonics, as depicted in figure 2.5. The maximum theoretical value that $a_w k_w$ can attain from gravity effects is 0.444 [1].

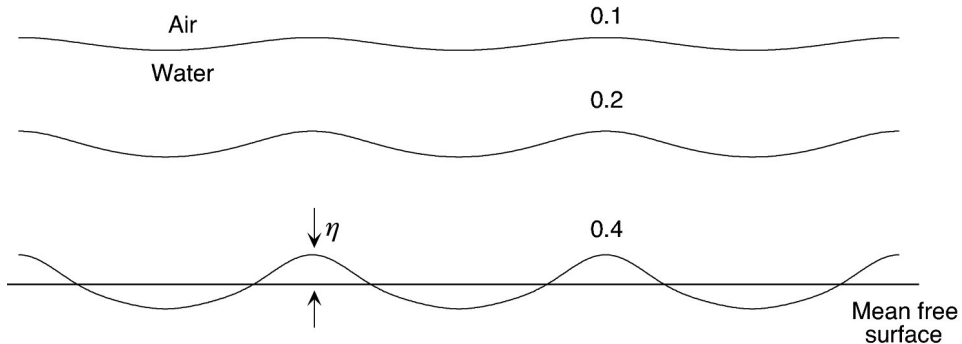


Figure 2.5: In this figure one can see the effects of three different values for $a_w k_w$. The vertical axis is exaggerated by 60% to make the effects clearer. Image courtesy of S. Martin[1].

If the wind adds more energy to the long waves the amplitude will increase until it breaks. When it breaks foam will be generated, and foam can make it complicated, or even pointless, to try to infer about the state of the ocean, based on radiation measurements alone. At any given time 2-3% of the ocean is covered in foam, an area about the size of the USA.

Further, it should be noted that natural or human-made surface slicks e.g. oil spills can change the physical dynamics of the ocean surface as well as its radiative transfer properties.

2.2.2 Electromagnetic radiation

Electromagnetic radiation or EMR is a complicated matter. It is also the pillar on which remote sensing relies on, thus this subsection seeks to give a short retort to the importance of electromagnetic radiation as well as an even shorter description of the phenomena through the lens of ocean remote sensing.

In quantum mechanics electromagnetic radiation propagates as photons; discrete bundles of energy with no mass, released by an atomic or molecular change of state. The energy carried by each packet can be described as follows.

$$\hat{E} = hf \quad (2.2)$$

Where h is the Planck constant ($h = 6.626 \times 10^{-34} \text{ J}$), and f is the frequency in Hertz. In applications, the EMR is described through the use of radiant flux Φ . Radiant flux is the rate at which energy is transported toward or away from a surface, given in watts. To properly define radiance, the unit of solid angle is frequently used, with the symbol Ω and an SI unit of steradian (sr). It is a two-dimensional angle in three-dimensional space that measures how large an object will appear from a given point or center. thus, the radiant intensity is given as $I = d\Phi/d\omega$, which is the radiant flux per solid angle. The flux density is given as $d\Phi/dA$. Combining all of these will result in a unit of measurements often used in remote sensing applications, the radiance L , with the unit of watts per square meter per steradian.

$$L \equiv \frac{d^2\Phi}{d\Omega dA \cos \theta} \approx \frac{\Delta^2\Phi}{\Delta\Omega \Delta A \cos \theta} \quad (2.3)$$

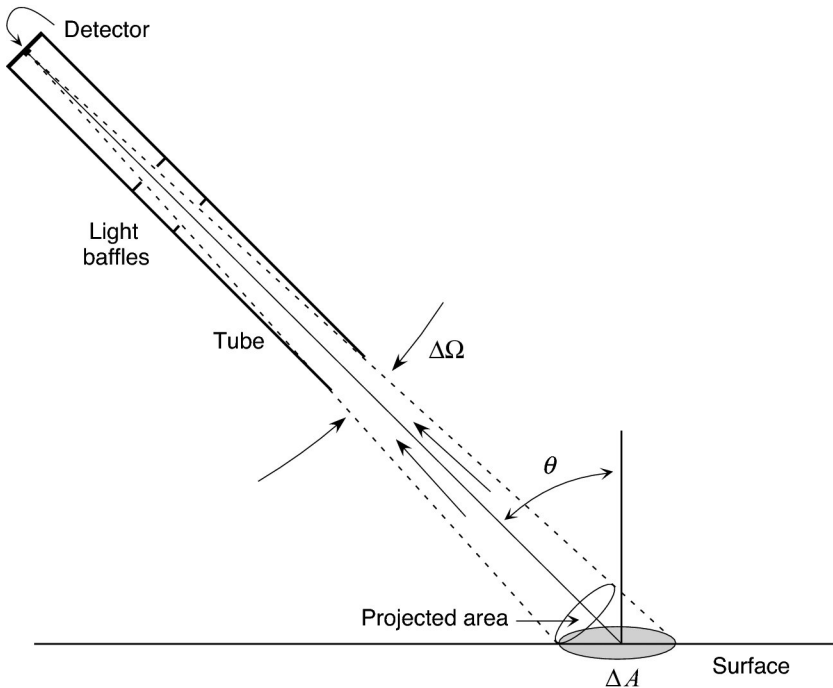


Figure 2.6: A schematic diagram of a instruments measuring the radiance of a given surface. Image courtesy of S. Martin [1].

The relationship is depicted in figure 2.6. This is a good way to quantify measurements for ocean remote sensing as several surfaces of oceanographic interest have radiances that are independent of look angle.

In many ocean remote sensing applications and algorithm descriptions the measurement is not given in radiance L , but rather in reflectance ρ , by the following relationship[12, 13], see the glossary

$$\rho = \pi L / F_0 \cos \theta_0 \quad (2.4)$$

To fully appreciate the effects of EMR one needs to have a comprehensive understanding of useful approximation approaches, definition and properties of radiating surfaces and what this means for a remote sensing instrument. This is outside the scope of this document, and is described in S. Martin *An introduction to ocean remote sensing* chapter 3 [1] or the *NASA ocean optics web book*[9].

2.3 Ocean Remote Sensing From Satellites

Remote sensing is to measure electromagnetic radiation from the ocean surface. In an effort to acquire information about the ocean, land, and/or atmosphere without being in physical contact with the object or phenomena under investigation[9, 14, 1]. Electromagnetic radiation, the topic of section 2.2.2, is a common measurement to infer information about the ocean from, but it is not the only one[1]. Since electromagnetic radiation is not a direct measurement, the properties of the physical phenomena under investigation need to be inferred from the intensity and frequency of the perceived radiation.

Due to atmospheric effects, the topic of section 2.4, there is only a few subsets of the electromagnetic spectrum (EMS) that is suitable for passive observation and monitoring of the ocean[1]. Passive remote sensing, as opposed to active remote sensing, is when the instrument or system does not provide any kind of illumination of the phenomena under investigation. The only illumination sources being often being the sun or the phenomena itself. The wavelength bands from ultraviolet, visible, infrared and microwave radiation are the bands most easily measured for satellite systems, and oceanographers are able to infer about the state of the ocean form these wavelengths in a meaningful way.

The wavelengths are illustrated in figure 2.2. In the visible part of the EMS, the topic of observation is often ocean color, the topic of section 2.5[9]. The infrared observations are mainly concerned with black body observations and sea surface temperature, and it is not dependent on the sun as an illumination source. To get good observations in the infrared part of the spectrum a cloud-free sky is needed. Infrared observations are also used for inferring about the atmospheric conditions and aiding in the atmospheric correction as well as being used for cloud detection[1]. the microwave bands are not as prevented by undesirable cloud coverage and can provide radiation data which enables one to infer about the salinity and sea surface temperature.

The NTNU SmallSat Program will be using a hyperspectral camera and is thus submitted to the spectral range of the visual to near infrared, as insinuated by section 2.1. The mission will be focusing on ocean color observations, as stated in the preliminary system description[5]. Although much of the mission is yet to be determined, preliminary reports suggest that the payload will have a spectral resolution of about 5nm, and be able to perceive wavelengths in the range of 400nm to 900nm, from the visible and into the near infrared.

2.3.1 Orbits for ocean remote sensing

There are a lot of considerations to take into account when deciding an orbit for a satellite. The space environment is hostile and harsh. There are phenomena such as solar storms, radiation pressure, gravitational perturbations, space debris, graveyard orbits and radio frequency interference[1]. All of this makes it quite difficult to do operations in space, but not impossible. For ocean remote sensing there are three common orbits i.e. geosynchronous, sun-synchronous and low-inclination orbit, as shown in figure 2.7 [1, 14]. Each remote sensing application is suited for a specific orbit. When the application is remote sensing for oceanographic observations it is commonplace to use sun-synchronous orbits, and they are often referred to as polar orbits[3]. This orbit is popular due to its many advantageous characteristics[5, 1]. The altitude of a polar orbit is around 800 km which enables a higher spatial and temporal resolution when compared to the altitude of a geosynchronous orbit at 35,800 km. A low-inclination orbit will be able to give an even higher spatial and temporal resolution with a typical altitude of 350 km, however, it will not be able to cover the entire Earth. A polar orbit will typically have an orbit period of 90 minutes and depending on the swath width of the sensor be able to cover the entire Earth in only a number of days[14]. With a polar orbital configuration, it is possible to map any desirable regions of the Earth with a considerable temporal and spatial resolution. Another advantage of the sun-synchronous orbit is the fact that the sun as an illuminations source will be available for a large part of the orbit cycle, and this is essential for ocean color observations. The NTNU SmallSat Program is opting for sun-synchronous / polar orbit [5].

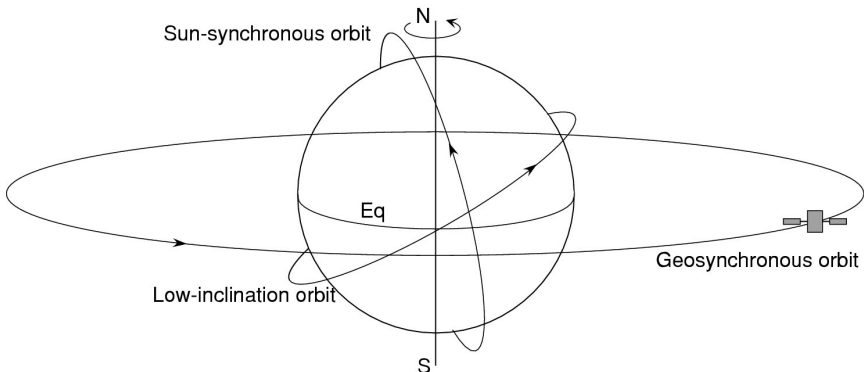


Figure 2.7: An illustration of the three most common orbits for remote sensing satellites. The Eq line denotes the equator, and the N and S denote the north and south pole respectively. Image courtesy of S. Martin [1].

2.3.2 Image acquisition for ocean remote sensing

There are nominally two methods used for observing the electromagnetic radiation from oceans in satellites. Namely whiskbroom- and pushbroom-scanners, as described in section 2.1.1. A depiction of a pushbroom scanner can be found in figure 2.4. A pushbroom scanner is able to take an image line by line, while a whiskbroom scanner complicates

this matter somewhat. The whiskbroom scanner operates by rotating its point of focus across-track whilst the instrument will be moving forward along-track, as depicted in figure 2.8. The main advantages of a whiskbroom scanner are the wide swath width and that they are usually equipped with some kind of calibration source, enabling them to be calibrated on every revolution of the instrument, when compared to a generalized pushbroom scanner. However, a whiskbroom scanner suffers from low spatial resolution and a low exposure time resulting in a worse signal to noise ratio (SNR), when compared to a general pushbroom scanner[1]. The NTNU SmallSat mission will be equipped with a pushbroom scanning hyperspectral camera, in part due to the reasons stated above [5].

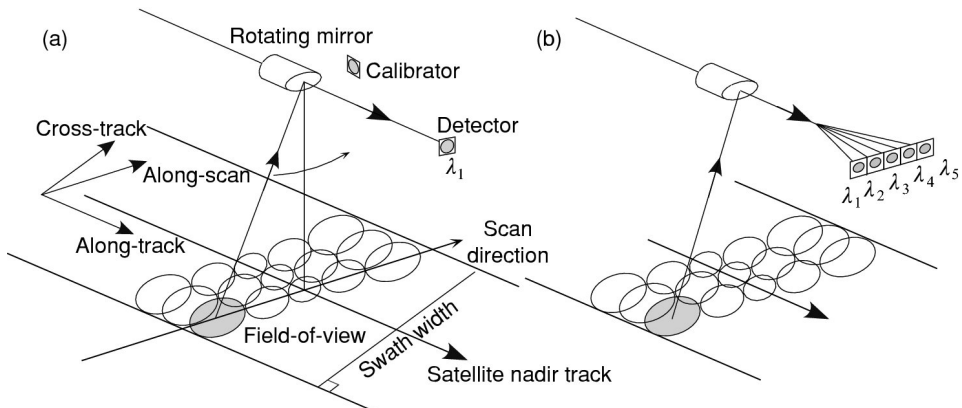


Figure 2.8: An illustration of a whiskbroom scanner. (a) is for a single wavelength, while (b) is for multiple wavelengths. Image courtesy of S. Martin [1].

2.3.3 Processing levels and archives

There are several levels of data products from Earth-observing satellites, and one can find several descriptions with some subtle differences in definition [14, 9, 1]. This section is meant to summarize the definition of each level as presented by NASA, arguably the most important provider of ocean remote sensing data, as described by the ocean color group at NASA [].

Level 0 data are unprocessed engineering outputs from the instrument at full resolution. Communication artifacts e.g. headers, duplicates, telemetry errors are all removed. This level is the rawest format available, and it is not common to provide users with data at this level.

Level 1A data are the preferred archive data. At this level, the data is at full resolution and still unprocessed, but annotated with ancillary information i.e radiometric and geometric calibration coefficients, as well as georeferencing parameters e.g. ephemeris data, computed and appended, but not yet applied. Thus the level 0 data can be perfectly recreated using level 1A data and no information is lost. The radiometric calibration coefficients mentioned here are to some extent the topic of this document.

Level 1B data are the Level 1A data with the radiometric calibration coefficients applied. Since certain appended data e.g. referencing parameters has not yet been applied it is customary that they too are appended at this level. This data is often presented in a more user-friendly manner, and it has been stated that science starts at Level 1B. Level 0 or Level 1A is not retrievable from this processing level.

Level 2 data are the Level 1B data processed into geophysical variables e.g. sea surface temperature, sea ice cover and of course different ocean color specific parameters. Level 2 data are obtained by correction for atmospheric effects, cloud masking and attenuation caused by water vapor. The corrected Data is then analyzed using an appropriate algorithm for retrieval of desired geophysical variables.

Level 3. At this level, the results from the previous data Level is mapped onto a well-defined spatial grid over an equally well-defined time frame. The areas of the spatial grid affected by external factors e.g. cloud coverage and differences in swaths are kept as is. That is when there is missing data it is presented as such in the spatial grid.

Level 4. At this level data from several sources are applied to augment the spatial grid of level 3. Measurements from several satellites and in-situ measurements are combined, and optimal interpolation schemes are applied, to produce a gap-free product on a uniform spatial grid, for a given time frame. The product may vary depending on the available measurements.

2.4 Atmosphere and Atmospheric Correction

The atmosphere greatly affects the transmission of radiation between the ocean and the satellite instrument[1] i.e. on the best of days the amount of radiance received from the ocean surface is approximately 10% of the total radiance transmitted[9, 15, 13, 1].

To describe the process of inter-calibration of satellite instruments, in particular, vicarious calibration, it is necessary to review the components of the atmosphere, or more specifically the atmospheric correction[15].

The atmosphere consists of many different components that interact with photons at different wavelengths in complex ways. The presence of gases in the atmosphere e.g. nitrogen, oxygen, carbon dioxide and ozone in fixed concentrations combined with the variable concentrations of water vapor limits the electromagnetic spectrum available for Earth observations. Effectively limiting the available spectrum to the visible through microwave range. Within this narrow band, the atmospheric absorption varies due to the varying concentrations of liquid water droplets, ice particles in the clouds and water vapor. Furthermore, the effects from the following constituents also affect the radiance received from the ocean greatly.

- aerosols and aerosol scattering
 - Small liquid or solid particles in the atmosphere radiance path
 - ionospheric free electrons
 - electrons in the ionosphere affected by solar-driven molecular disassociation.
 - molecular absorption, emission and scattering
-

-
- Discrete emission and absorption by molecules through a change in quantized energy state, and the resulting scattering of radiative signals i.e. deviation from a straight path trajectory due to non-uniformity in the medium of which it has passed through.
 - atmospheric attenuation
 - The gradual loss of flux intensity as the photons pass through several layers of the atmosphere.

A good resource to better understand the atmosphere and the ocean-atmosphere interface can be found in chapter 4 and 5 of S. Martin *An introduction to ocean remote sensing* [1], or the tenth IOCCG report[16]. A simple illustration of the atmosphere and its layers can be found in figure 2.9

There exists several algorithms or approaches to perform atmospheric correction at a remote sensing ocean color satellite[16]. In the following paragraph the standard algorithm deployed by NASA Ocean Biology Processing Group (OBPG) will be presented, as adapted from [13, 15]. The approach depicted in [15] is of particular interest as it is a sensor independent approach to vicarious calibration. This approach depicted here is expressed using radiance, but in the original paper [13], it is expressed using reflectance. The relationship between reflectance and radiance is shown in equation 2.4, and its calculation is trivial given the extraterrestrial solar irradiance and the solar zenith angle. The total radiance L_t is given as follows, not accounting for observations with sun glint contamination, noise or other shortcomings of the instrument:

$$L_t(\lambda) = [L_r(\lambda) + L_a(\lambda) + t_{d_v}(\lambda)L_f(\lambda) + t_{d_v}(\lambda)L_w + t_{d_v}(\lambda)]t_{g_v}(\lambda)t_{g_s}(\lambda)f_p(\lambda) \quad (2.5)$$

For definitions see the glossary. All terms can be reliably estimated given the radiant-path geometries and measurements of atmospheric pressure at the surface with the expectations of the water leaving radiance L_w and the radiance contribution due to aerosols and Rayleigh-aerosol interactions L_a . However, due to the high absorption and weak reflectance from near-infrared wavelengths over open clear oceans the contributions from the water leaving radiance can be neglected i.e. $L_w \approx 0$ and the aerosol effects can be estimated from the total radiance received, both for the case of single scattering and multiple scattering. If the total radiance at two different near-infrared wavelengths is available these measurements combined with aerosol models can be used to determine the type and concentration of aerosols for all wavelengths in the acquired image. When L_a is retrieved the equation only contains one unknown, the water leaving radiance L_w , and it can then be retrieved easily. The next step in the process would be to determine the normalized water-leaving radiance $L_{wn}(\lambda)$, the fundamental measurement that forms the basis for all derived products associated with ocean color.

$$L_{wn}(\lambda) = L_w / \mu_s f_s t_{d_s} f_b f_\lambda \quad (2.6)$$

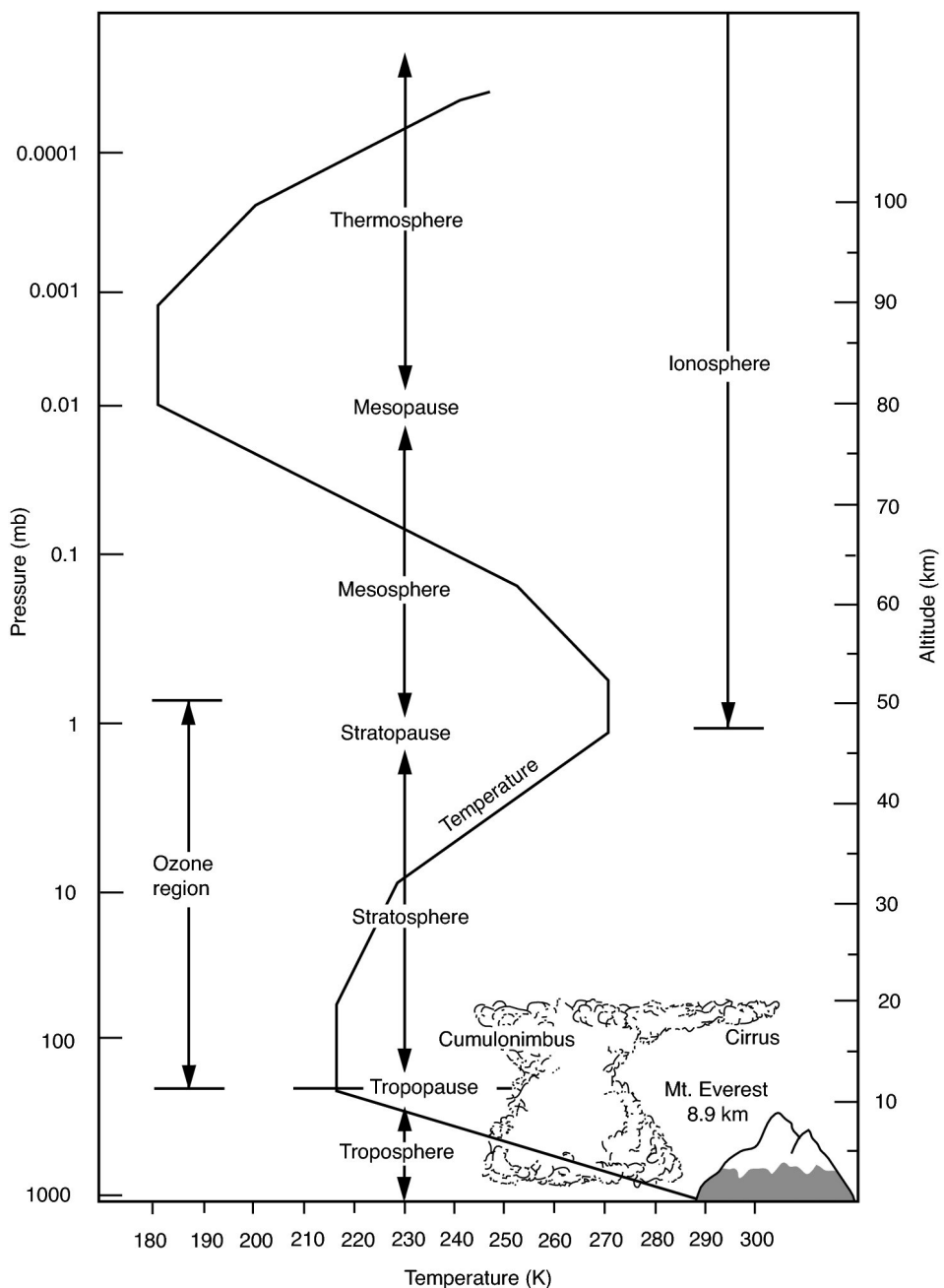


Figure 2.9: A nice illustration of the atmosphere. Showing the different layers and some of the properties associated with a given altitude. Adapted from S. Martin [1].

This procedure is also reiterated in greater detail in chapter 6 section 5 of [1], using a slightly different approximation of radiative transfer properties and notation, as well as in the papers referenced above.

Ocean remote sensing has until recently been mainly focused on multispectral instruments and multispectral algorithms[17]. There is, however, a great need for atmospheric corrections when measuring in the hyperspectral domain as well, and it exists some preliminary results for this[18, 19, 20, 21, 17]. The hyperspectral algorithms mainly differ from traditional multispectral atmospheric correction by utilizing some sort of spectrum matching rather than the traditional ratio-based, NIR-focused approach.

2.5 Ocean Color

The objective of many ocean remote sensing satellites or instruments is to infer about the state of the ocean derived from ocean color measurements. Measurements of radiation from the ocean in bands associated with visible and near-infrared wavelengths, $\lambda \in [400nm, 2000nm]$, falls within the topic of ocean color [9]. This is currently both the spectral domain and objective associated with the NTNU SmallSat Program[5].

Ocean color remote sensing, also known in as ocean color radiometry, has many societal benefits[22, 1, 9]. Observations of ocean color are currently used in such applications as mapping of chlorophyll concentration and biological research to better understand maritime biology and dynamics. Furthermore, it is used extensively in climate studies, fisheries management, mapping of ocean structures, monitoring of water quality for recreation and detection of harmful matter in the oceans. In ocean remote sensing terminology there are two classification types for ocean waters. The types of water are Case 1 type water and case 2 type water[16, 23]. In case 1 type water scattering mainly arises from organic material i.e. phytoplankton, and it is mainly open ocean scenes that are classified as type 1. The scattering from case 2 type waters is predominantly a result if scattering from inorganic material, and coastal ocean scenes are mainly classified as type 2. It should be noted that this classification concept is flawed in the sense that all oceanic waters contain elements belonging to both descriptions[24]. However, It is a useful distinction to make in order to identify what your instrument should be looking for and what your instrument will be able to see.

The ocean plays a great role in all life on Earth and constitutes most of the Earth surface, yet it is the least explored of all of Earth's environments. Ocean color remote sensing by satellites has during the past forty years revolutionized the way we can monitor the ocean spatially and temporally. Although the origin of this endeavor has its roots in research, operational ocean color remote sensing is of utmost importance to society[22].

2.6 International Efforts for Earth Observations

For the measurements from Earth observing satellites to be valuable to a scientific community it needs to adhere to certain qualities[1, 25]. As the space environment can be quite harsh (see section 2.3.1), degradation of a system or instrument in space is to be expected [26, 12]. Any instrument going to space has to go through rigorous testing i.e. a spectral camera will be calibrated against known standards over a longer period of time (usually) before ever being instrumented on a satellite.

There exists currently an abundance of organizations working towards a more unified utilization of Earth observation data. For ocean color applications the Ocean Biology Processing Group has since the launch of the conceptual coastal zone color scanner (CZCS) in 1978 laid the groundwork for how to obtain data records with a sufficient accuracy with respect to ocean remote sensing. Furthermore, organizations such as *Quality Assurance for Earth Observations* (QA4EO) led by the committee on Earth Observation Satellites (CEOS) tries to make a universal framework for quality assurance. The objective of CEOS is to ensure international coordination of civil space-based Earth observation programs e.g. ESA and NASA programs. Furthermore, CEOS promotes any effort to make data more accessible in an effort to maximize the societal benefit and to map the road to a more prosperous and sustainable future for humankind[27]. Furthermore, The International Ocean Color Coordinating Group (IOCCG) is working more specifically towards ocean color applications, with similar objectives to that of CEOS. The vision of IOCCG is to make ocean color data and analysis known and accessible to as many people as possible. Through this engaging oceanographers and scientists all over the world. The most relevant objective of the IOCCG for this documents would be their effort to optimize the quality of data for calibration and validation i.e. encourage the formation of an international calibration and validation network for ocean color and ensure that sea-truth measurements conform to accepted international protocols and traceable standards. An ongoing project for the IOCCG is to facilitate the formation of a distributed calibration and validation archive and database network [28, 12].

The contributions made by the IOCCG is invaluable to any program that seeks to explore the ocean. Thus, the information put forth by the IOCCG, both in form of reports, in form of training courses and other forms of information are contributions that make ambitious programs e.g. the NTNU SmallSat Program possible and the data gathered from such programs useful beyond technology demonstrations.

In-flight Calibration and inter-calibration of Satellite instruments

3.1 Calibration & Validation

There is a great need for post-launch calibration of satellite instruments in order to obtain useful data records [14, 6, 9, 29, 30, 31, 15, 1, 13, 12]. The subsequent sections and chapters are mainly concerned with radiometric calibration of some sort, with a vicarious calibration taking the lion's share of the focus. The following section is strongly based on the structure of the paper titled *Overview paper on inter-calibration of satellite instruments* by G. Chander et al. [29], and by the IOCCG *In-flight Calibration of Satellite Ocean-Colour Sensors* report[12].

3.1.1 Definitions and Requirements

It exists nominally two approaches for expressing the measurements from ocean remote sensing[12], namely Radiance-based and reflectance-based. For the ideal sensor, a Radiance-based calibration approach would be to calibrate according to a radiating object, whilst the reflectance-based approach would be to calibrate according to the reflectance from an illuminated object.

The digital number associated with level 0 data, when regarding the radiance-based approach, can be expressed as follows:

$$V_c(\lambda) = k_L(\lambda)L_c(\lambda) \Rightarrow V(\lambda) = k_L(\lambda)L(\lambda) = \frac{V_c(\lambda)}{L_c(\lambda)}L(\lambda) \quad (3.1)$$

Where V is the voltage or digital number, k is the coefficient, L is the reflectance and the subscript c denotes calibration or calibration source.

The reflectance-based approach is more complicated, see figure 3.1 for illustration in combination with equation 2.4.

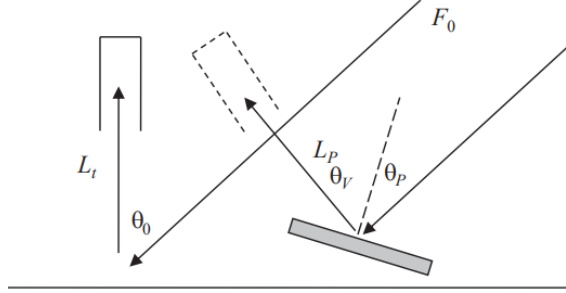


Figure 3.1: A schematic drawing describing reflectance

If the sensor views a scene solely illuminated by an irradiance E it could be expressed in the following way:

$$V(\lambda) = k_L(\lambda)\rho(\lambda)E(\lambda)/\pi \quad (3.2)$$

Furthermore, given that we had a Lambertian reflector $R_p(\theta_v, \theta_p)$ i.e. a surface where the apparent brightness is the same regardless of viewing angle. R_p defined to be the power per unit area reflected divided by the area illuminating the plate, with illumination irradiance E_p . Note that the function R_p is determined through sensor/camera characterization. The voltage of the sensor from the received radiance at the sensor would be expressed as follows:

$$V_p(\lambda) = k_L(\lambda)R_p(\lambda)E_p(\lambda)/\pi \quad (3.3)$$

thus, from combining equation 3.2 and 3.3 and assuming that the irradiance stays the same i.e. $E(\lambda) = E_p(\lambda)$, the case when using a reflectance plaque in your sensor, you would get the following expression:

$$V(\lambda)/V_p(\lambda) = \rho(\lambda)E(\lambda)/R_p(\lambda)E_p(\lambda) \quad (3.4)$$

$$V(\lambda)/V_p(\lambda) = \rho(\lambda)/R_p(\lambda) \quad (3.5)$$

This reflectance plaque would take up physical space and it would degrade over time. This degradation can be counteracted by onboard calibration techniques i.e Lunar and Solar calibration.

After the initial success of the proof-of-concept mission coastal zone color scanner (CZCS) in 1978 [13, 12, 25] NASA OBPG was able to predetermine the necessary requirements of ocean color remote sensing satellite sensor to be successful. The uncertainty in the water leaving radiance cannot exceed 5% in oligotrophic waters i.e. water environments with little to no nutrients or dissolved matter to disturb the signal at $\lambda = 443nm$. Even

given an atmospheric correction close to perfect this would demand a radiometric calibration coefficients with uncertainties no higher than 0.5%. This is difficult to achieve even under pre-launch conditions, and thus the need for in-orbit calibration and calibration adjustments i.e. vicarious calibration is necessary. In concept, adjusting the calibration coefficients is a simple task.

Vicarious calibration can be divided into two categories i.e. radiometric vicarious calibration and system vicarious calibration. The goal of any form vicarious calibration is to successfully determine the correct response of $k_L(\lambda)$ after launch. Radiometric vicarious calibration is defined as estimating the TOA radiance or reflectance and comparing that to the measured. This calibration approach is limited by the accuracy of surface measurements.

System vicarious calibration is defined as a calibration of the combined sensor response and atmospheric correction algorithm. Since the atmospheric correction is based on some of the NIR-bands the biggest caveat of this approach is the fact one assumes no error in the highest NIR-band, following the approach touched upon in section 2.4. However, the system calibration approach has many advantages when compared to radiometric calibration e.g. the residual calibration errors will be reduced from the in the VISNIR range, the residual errors will be of the same sign and perhaps most significant the sensor is forced to do the job it was designed to do.

The two approaches can be expressed in the following way, with the t denoting targeted measurements. see the glossary.

$$g_{radiometric} = \frac{L_t^t(\lambda)}{L_t(\lambda)} \quad g_{system} = \frac{L_w^t(\lambda)}{L_w(\lambda)} \quad (3.6)$$

3.1.2 General Calibration Problems

There are several pitfalls regarding how to be able to validate the measurements made by remote sensing systems[29].

Traceability refers to an unbroken chain of comparisons between an instruments measurements and a known standard. This will in return be used to determine the instruments bias, precision, and accuracy, which is important to adhere to the requirements of CEOS and IOCCG (see section 2.6). In practice it is difficult or impossible to have a *unbroken chain* of comparisons for a remote sensing satellite from pre-launch to launch and after becoming operational. To lessen this problem it is common to regularly compare measurements of pseudo-references e.g lunar observations as a substitute for irrefutable national standards.

Furthermore, the sampling differences of different ocean remote sensing sensors will make direct comparisons a rare opportunity. Independent sensors will most likely not have identical spectral or radiometric resolution, nor will they necessarily sample the same spectral bands or at the same spatial resolution.

Scene variability will also pose a great difficulty regarding comparisons. The surface reflectance of a scene may be highly dependent on viewing geometry, time of year and other atmospheric conditions.

Lastly, instrument capabilities and the choice of reference instrument will greatly impact the results of comparisons. CEOS and other similar initiatives provide metrics that to

some extent quantify the quality of a measurement that could be used for inter-comparison. The quality of such measurements should be taken into account when doing comparisons and recalibration of an instrument.

3.2 On-board calibration techniques

3.2.1 Lamp Calibration

It common to use a lamp e.g. a tungsten lamp as an internal light source in ocean remote sensing system for on-board calibration[12]. Tungsten is used due to its low energy requirement and precise emission spectra.

A lamp will degrade over time due to the harsh space environment i.e. this calibration method will only enable monitoring of the sensitivity of the system over time. This calibration can then be viewed as relative, meaning that the traceability and repeatability can be checked wrt. time, but not wrt. to a known source or standard.

For a small satellite, the available space will be restricted i.e. fitting a calibration lamp inside it, combined with the potential mechanical movement to periodically check the lamp when using a push-broom scanner, will have a high risk and a high cost. Thus, this approach is not ideal for the NTNU SmallSat Program[5]. Furthermore, internal light sources, as the only solution, for calibration of an ocean remote sensing sensor is insufficient, and other approaches are needed in addition to getting adequate stability.

3.2.2 Lunar Calibration

In most forms of literature regarding ocean remote sensing calibration, lunar calibration is mentioned in one form or another. The irradiance of the moon can be modeled quite accurately, accounting for variations in brightness due to phase angle, nonuniform albedo, distance, and lunar librations[29]. A standard model for this is the ROLO model provided by the Robotic Lunar Observatory in the U.S. [32]. There has also been made attempts to improve this model[33, 34].

Using lunar observations for calibration will provide the system with a stable calibration source. If possible, most ocean remote sensing systems routinely scan the moon surface. Due to the moons stability, intercomparison between different measurements is independent of time. Furthermore, the moon has the same radiance as the ocean i.e. there is less concern regarding saturation of an instrument designed for ocean observation according to S. Martin *An Introduction to Ocean Remote Sensing*[1]. However, other sources raise concerns regarding the brightness of the moon saturating an instrument designed for ocean color observations [29, 12].

Certain requirements will arise from performing lunar calibration[12] e.g. a larger spacecraft maneuver, the need for a photometric model such as ROLO and there will only be one to two opportunities to perform this calibration per month. However, the largest caveat of this approach with respect to the NTNU SmallSat Program is the fact that one would need to capture the entire moon in one image to tie the measurements to a model like ROLO. This is seldom feasible given the limiting swath angle of a push-broom scanner, and for this reason satellites such as MERIS is unable to perform on-orbit lunar calibration.

Lunar calibration is the best choice for monitoring relative temporal gain trending. However, it would not be the first choice for absolute calibration, but it should be noted that many satellites use the moon for calibration, thus enabling for intercomparison of measurements with potentially well-calibrated instruments.

3.2.3 Solar Calibration

Reflectance-based radiometric calibration using the sun as a light source can provide good absolute radiometric calibration in the VISNIR bands, and is one of the best resources for this[35]. Carefully designed solar diffusers i.e. a plaque that scatters light in some manner, such as Space-Grade Spectralon [36, 12], allow for calibration providing full pupil, full optical path, and full field of view radiometric calibration for push-broom scanners. Current diffusers being developed can be viewed as fully Lambertian reflectance surfaces ($> 99\%$), but they will degrade over time. Due to the degradation of a solar diffuser, they will only be able to discover abrupt changes in radiometric sensitivity[1] and not absolute changes.

To fully utilize this approach one needs to characterize the bidirectional reflectance function associated with the diffuser plaque. During calibration, the plaque will be illuminated by a solar flux proportional to the square distance between the sun and the Earth. The sun has a seasonal variation of 1% wrt. irradiance. Both the sun-Earth distance and the solar irradiance can be assumed to be well known[12], in combination with the well-known Earth-satellite position and the attitude of the satellite, allows for precise computation of calibration geometry. Thus, the main sources for uncertainty when considering reflectance-based calibration using solar observations are limited to the accuracy of the spectral response function $k_L(\lambda)$ and the accuracy of the bidirectional reflectance function for the diffuser plaque.

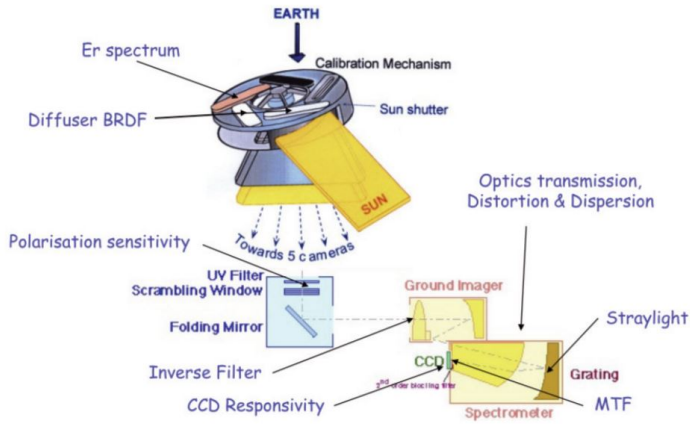


Figure 3.2: Diagram of the MERIS on-board calibration hardware. Image courtesy of IOCCG[12].

Again, for a small satellite system, the available space will be restricted i.e. fitting a diffuser plaque inside it will have a high cost. Furthermore, this approach would require

attitude changes in the spacecraft, and one would also need to differentiate between looking at the Earth with the optics and looking at the sun (See figure 3.2. Thus, this approach is not ideal for the NTNU SmallSat Program[5].

3.3 Calibration Using Naturally Occurring Phenomena

Vicarious calibration methods are used either alternatively in the absence of onboard calibrators or to check the onboard calibration device. As was hinted at during section 3.2, the accessibility for traditional onboard calibration for small satellites using a push-broom scanner is somewhat limited. In other words, the need for vicarious calibration is evident. The following approaches determine the relationship depicted in equation 3.6, thus implying that you go backward in estimating the radiance at TOA e.g. calculate $L_t^t(\lambda)$ and compare to the radiance measured, see equation 3.6.

3.3.1 Pseudo-Invariant Calibration Sites

Certain areas on the globe with large homogeneous composition on the surface are well suited and quite popular for calibration[37]

The use of predetermined, stable and homogeneous desert sites allows a wider applicability of such comparisons through a bidirectional and spectral characterization of the surface reflectance of the site[12]. The sites monitored by CEOS in one fashion or another is depicted in figure 3.3, combined with some common ocean remote sensing specific system calibration sites[27, 38, 15]. The sites were selected due to their spatial homogeneity and size, temporal stability across seasons, low cloud cover and low precipitation. At the sites marked with a red star, the site is also monitored at the ground level, thus enabling for system calibration as well.

One challenge using this approach for a satellite designed for ocean remote sensing is the brightness of the sites when compared to the brightness of the ocean.

3.3.2 Deep Convective Clouds

A deep convective cloud, often abbreviated to DCC, is a bright cloud with interesting features for remote sensing e.g. naturally being a nearly perfect solar diffuser and close to being a perfect Lambertian surface providing a simple bidirectional diffusion function[29]. furthermore, DCCs have a seasonal migration following the sun, an inherent high signal to noise ratio and a nearly flat spectral response, all features which makes them well suited for on-orbit calibration[39]. These clouds occur naturally at a very high altitude, often above 80% of the air, 99% of the atmospheric water vapor and above 100% of aerosols in the troposphere. Thus, DCCs are free of the uncertainties that these atmospheric constituents often bring. Calculation of the radiance at TOA is done using the look-up tables associated with the parameters that need to be estimated and appropriate band responses, etc, well described in [12].

These clouds often have a large spatial extent both vertically and horizontally, and can reach heights or thickness in the order of magnitude of 10,000 km[40]. DCCs mostly

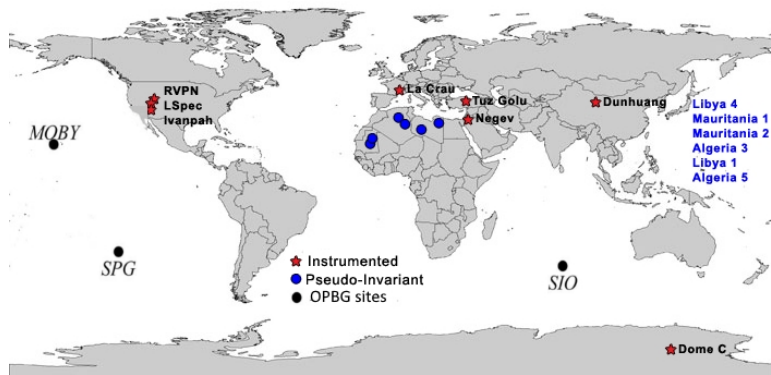


Figure 3.3: Map of Pseudo-Invariant Calibration Sites controlled by CEOS and the operational sites used by NASA OBPG. Image adapted from CEOS and OBPG [27, 15].

occur in tropical areas, and they have been proven to be good invariant targets for vicarious calibration in the VISNIR bands[41, 39, 34]. For bands longer than the VISNIR bands, properties of DCCs becomes dependent on temperature [41]. They are, however, considered to be very stable in the VISNIR range. The reflectance coming from DCCs in VISNIR bands is mainly a function of the optical depth of the cloud, and this can be accurately estimated using NIR bands[12].

Using the radiance measured and during the night combined with the ROLO irradiance model, after applying strict criteria wrt. spatial and brightness temperature homogeneity, it is possible to do indirect lunar observation garnering decent results[34].

The biggest challenge regarding calibration using DCCs is due to their excessive brightness, which for sensors designed for ocean color may lead to saturation. These targets are even brighter than PICS.

3.3.3 Rayleigh Scattering

Rayleigh scattering is the main source of incident solar irradiance measured at TOA, especially in the visible bands. in addition to this, it constitutes 90% of the signal at TOA for the visible bands[29].

When calibrating using Rayleigh scattering it would be beneficial to acquire images where secondary atmospheric effects e.g. aerosol scattering, scattering from the water body, gaseous absorption or reflection form whitecaps are minimized. These secondary effects can, however, be estimated to some extent using radiative transfer models, resulting in an accuracy of approximately 2-3% (depending on the wavelength) of the estimated TOA[12, 16, 1]. It is not necessarily a stable source for calibration, but its radiative properties are well understood and well modeled.

The biggest advantage of this approach is that the calibration is not limited geographically

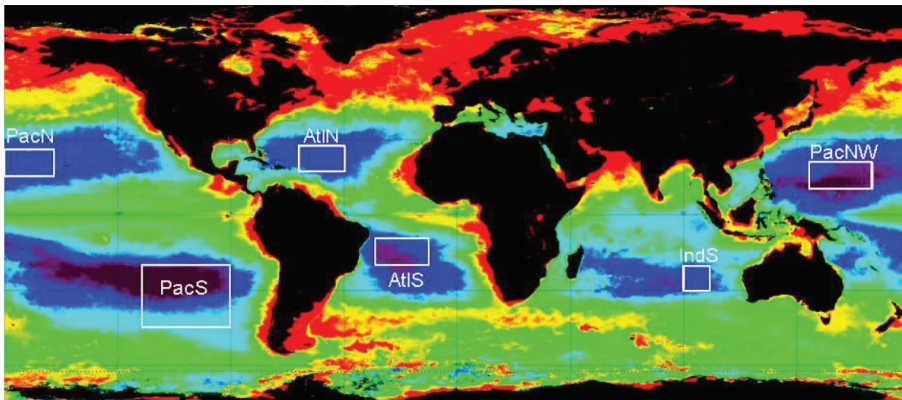


Figure 3.4: Map of Areas recommended for calibration via Rayleigh Scattering. The areas are inside the boxes. Image courtesy of Bertrand Fougne, CNES.[42]

or geo-physically. Another interesting feature wrt. ocean remote sensing is that the pixels in question do not have a high brightness. In other words, this approach is ideal for instruments that are in danger of saturating, compared to calibration using desert sites and deep convective clouds. Furthermore, this approach provides both absolute calibration and monitoring of gain coefficient trending. Rayleigh scattering also provides a source for inter-calibration as the sites depicted in figure 3.4 could be used for inter-calibration of satellite instruments. However, a large dataset of observations is needed to get good results and it is not trivial to select well-suited pixels.

3.3.4 Sun Glint

Sunglint from the ocean provides a source of spectrally flat high reflectance, especially for the longer wavelengths in VISNIR[29]. However, using the sun glint for calibration is not trivial. The received reflectance is dependent on observation geometry and ocean surface roughness, which there exist good models for [43]. For these models, the largest uncertainty is the wind speed, which can be difficult to determine[12].

Sunglint observations are inherently bright, which may cause saturation problems for many sensors designed for ocean color observations. This problem can be mitigated using pre-selected ocean sites, which in practice usually correspond to the same sites as in figure 3.4. Furthermore, a meticulous choice of scanning geometry to reduce brightness should be applied. In addition to this the need for ancillary data e.g. ocean surface pressure, ocean surface wind speed and measurements of the total ozone amount, further promotes utilizing simultaneous observation opportunities.

As a result, sun glint observations are not well suited for absolute calibration. It is on the other hand well suited for inter-band calibration, given a reference band, and the results from inter-band comparison can in return be used to propagate the results from absolute calibration to all bands.

Table 3.1: An overview of frequently and potential suitable reference locations used for system vicarious calibration of ocean remote sensing satellites. See figure 3.5 for location. Adapted from Zibordi et al. [44].

Acronym	Region	Lon	Lat	Notes
SPG	South Pacific Gyre	-125.0	-25.0	Virtual site
NPO	North Pacific Ocean	-157.8	19.4	Near the MOBY Site operated by NOAA
MSea	Mediterranean Sea	25.0	34.0	Potential site near Crete Island
CSea	Caribbean Sea	-67.0	17.5	Potential site near Puerto Rico Islands
ASea	Arabian Sea	72.0	10.0	Near the Kavaratti Site operated by ISRO
NAO	North Atlantic Ocean	-28.5	39.0	Potential site near Azores Islands
LSea	Ligurian Sea	8.0	43.5	Near the BOUSSOLE Site operated by LOV
EIO	Eastern Indian Ocean	114.5	-32.0	Potential site near Rottnest Island

3.4 System Absolute Calibration

The approaches in section 3.3 is mainly well suited for radiometric calibration, but to get sufficiently accurate measurements wrt. ocean color applications, system vicarious calibration is required[12]. system vicarious calibration is essential to achieve the required accuracy of water-leaving radiance to be used for science applications [12, 15, 44]. Even if assuming perfect atmospheric correction, the absolute radiometric calibration would have to be accurate to a fraction of 1%. This is not achievable by any purely radiometric vicarious calibration method, or for that matter, in a laboratory pre-launch [12]

In system vicarious calibration the atmospheric correction scheme and instruments response are not considered separately. Thus the chosen atmospheric correction algorithm is important for the results. For this reason, the choice of calibration site is of great importance, and some sites worth considering are depicted in figure 3.5, and table 3.1. The sites are chosen due to their high spatial homogeneity i.e. mesotrophic or oligotrophic, waters with low levels of productivity[45], maritime aerosols, lack of any nearby land and otherwise high environmental stability. The sites are more suited than desert sites for ocean color sensors wrt. brightness and such.

The algorithms to perform the system vicarious calibration is in concept similar to the algorithms associated with radiometric vicarious calibration. As the targeted TOA radiance L_t^t is estimated using auxiliary measurements at the acquisition site and compared to the measured TOA radiance L_t , for the system vicarious calibration the water leaving radiance L_w^t is measured using a highly accurate spectral instrument[46] e.g. MOBY, BOUSSOLE and compared to the the estimated water leaving radiance by the system L_w . Thus, adjusting both the atmospheric correction algorithm and the sensor. Usually, the normalized water-leaving radiance $[L_w^t]_N$ and $[L_w]_N$ is used such that the comparison is not dependent on viewing geometry.

It is, however, a time-consuming process to gather sufficient amounts of data to do a satisfactory system vicarious calibration[12], e.g. it took NASA OPBG 2-3 years to obtain a sufficient number of samples at the MOBY site for system vicarious calibration of Sea-

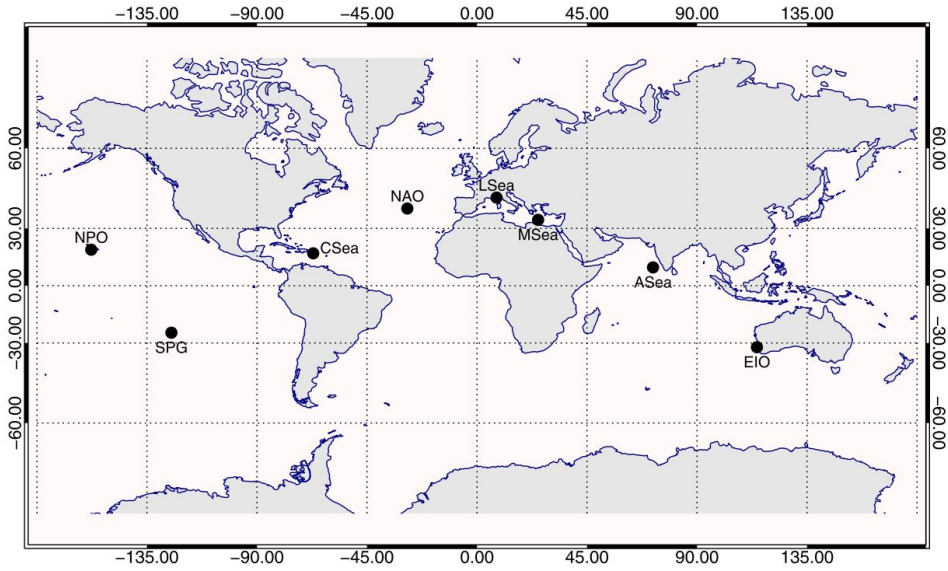


Figure 3.5: A map of frequently and potential suitable reference locations used for system vicarious calibration of ocean remote sensing satellites. Image courtesy of Zibrodi et al. [44]. See table 3.1 for information.

WiFS [15]. This being samples that were not contaminated in any way with undesirable or "hard-to-model" secondary atmospheric effects. In practice, the radiometric calibration in the shorter infrared band is then adjusted such that the expected aerosol model at the calibration site is retrieved correctly by the atmospheric correction scheme.

Furthermore, atmospheric correction algorithms deployed by NASA OBPG is highly dependent on the NIR bands, and this could be troublesome due to preliminary results suggesting relatively low SNR values in the NIR bands for the NTNU SmallSat Program when compared to other missions[17, 5, 15].

3.4.1 Other approaches

There exist more calibration strategies than what has been presented here[29, 12]. In this document the strategies of special interest wrt. ocean color remote sensing and the NTNU SmallSat Program has been emphasized. Some of the more notable methods not presented are star monitoring, the use of liquid water clouds, numerical weather predictions and direct applications of radiative transfer models.

Furthermore, this document has not been concerned with spectral calibration, another important matter for any operational ocean color sensor[12, 30]. A problem lessened through an elaborate choice of a diffuser, monochromators, observations of oxygen A-band or Fraunhofer lines i.e. atmospheric phenomena with distinct and sharp spectral characteristics, or through models of the spectral response of the instrument. Spectral stability is of particular interest to push-broom scanners with relatively high spectral resolution e.g. MERIS or HICO.

Chapter 4

Experiences From Historical and Current Ocean Remote Sensing Systems

Due to the empirical approaches used in most of the existing ocean remote sensing satellites it may be useful to take a look at former and existing platforms[1, 3, 12], and how these have handled problems such as inter-calibration, generating valuable data records and surviving in space. All satellites in this section were designed for ocean color monitoring and have/had polar orbits (with the exception of HICO being situated on the International Space Station or ISS).

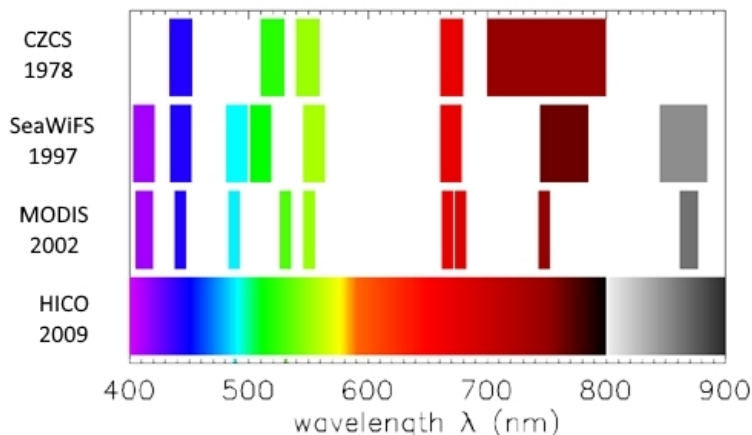


Figure 4.1: An illustration to compare some of the spectral ranges available for some of the instruments in this section. Image adapted from [9]

4.1 Hyperspectral Imager for Coastal Oceans

4.1.1 Mission and instrument

The Hyperspectral Imager for the Coastal Oceans, abbreviated as HICO, was a Remote sensing instrument situated on the International Space Station (ISS) launched 10. September 2009 That used a push-broom scanner[31]. At the time of its launch, the HICO system was the first spaceborne imager with a hyperspectral sensor specifically designed for coastal oceans[47], thus it was first and foremost an experimental mission. HICO had a nominal spectral range of 350-1080 nm, and an SNR above 200 to 1 in the spectral range of 400-700nm for in the VISNIR range[48], i.e. the laboratory characterization of the sensor met or exceeded the design parameters necessary to meet the demanding requirements that ocean color hyperspectral imaging imposes. Having a hasty (short, quick) development-to-launch schedule, it was not possible for the HICO mission to do an as precise testing of the instrument before launch, as is customary for equipment going into space. The kind of testing, where the instrument is calibrated and re-calibrated over a longer period of time in an effort to better characterize the instruments expected behavior and potential biases or drifting. It is important to remember that the HICO mission was only meant as technology demonstration [47], and not as an alternative to other more operational sensors e.g. MERIS.

4.1.2 Problems and Vicarious Calibration

The HICO instrument was not equipped with any onboard radiometric (or spectral) calibration devices nor was it able to utilize solar or lunar-based measurements as it was a rigid construction aboard the ISS. Implying that vicarious calibration was necessary to calibrate and validate HICO images if it was ever going to generate valuable data records[30]. Fortunately, the HICO instrument was able to acquire scenes a lot brighter than what an ocean color sensor is required to do without saturating i.e. use CEOSS sites for vicarious calibration. This was, of course, used extensively to moderate the initial problems that HICO experienced, utilizing simultaneous nadir overpasses with well-calibrated satellites e.g. MODIS and MERIS [30].

Somewhere between the radiometric calibration carried out in the laboratory on the HICO sensor and its installment on the ISS, the sensor lost approximately 25 % of its radiometric sensitivity. The causes for this are, as far as any documentation go, still unknown[30]:

We did suspect that the surface areas of the HICO front optical lens might be contaminated in the ISS environment. Therefore, arrangements were made to take high spatial resolution digital camera images of the HICO lens surface areas using one of the external manipulating arms on ISS. The resulting digital camera images demonstrated that the HICO lens surface appeared to be perfectly clean. Thus, at present, HICOs post-launch loss of radiometric sensitivity remains a mystery.

Furthermore, there was a lateral shift between the spectrometer and the camera of about $70 \mu\text{m}$ in the spatial direction and about $8 \mu\text{m}$ in the spectral direction. Resulting in parts

of the spectral and spatial domain being useless. This was discovered and resolved through spectral analysis of the oxygen absorbing bands[30] and comparing it to simulations.

As the biggest problem that the HICO mission experienced was caused by windows, one might consider opting for a purely UNIX based system in the future[31]:

The HICOs biggest problem on orbit is with single-event upsets affecting the HREPs computer, which is a PC running the Windows operating system. The computer locks up and must be restarted about once every three days of operation. Discussions with NASA personnel indicate that this is the typical performance for PCs, of which there are many on the ISS. The downtime resulting from these lockups causes the HICO to miss, on average, about one in five of its planned scenes.

4.1.3 Heritage

The HICO was not able to restart after being hit by a solar wind 13. September 2014[17]. At its core the HICO system has some interesting similarities when compared to the NTNU SmallSat Program[5] e.g.

- A philosophy of being a simplistic system made up by off-the-shelf, or easily obtainable components, in an effort to reduce development costs both temporally and financially.
- Being equipped with a hyperspectral push-broom camera
- Being made (in cooperation with NASA) at a university
- Being designed for ocean color applications

In many documents, the HICO instrument is stated to have a relatively high SNR in the visible range. The instrument did, however, struggle with a low SNR in the NIR range, making atmospheric correction unreliable [31, 17, 48].

Furthermore, it is, in general, an interesting case study regarding the use of hyperspectral images for ocean color wrt. the upcoming NASA PACE mission and similar hyperspectral missions [3, 17, 1, 49]. Showing many of the applications, not possible with traditional multispectral remote sensing [50].

4.2 MEdium Resolution Imaging Spectrometer

4.2.1 Mission and instrument

MERIS was a remote sensing instrument aboard ESA's Envisat Platform [51]. The instrument consisted of five cameras, positioned side-by-side in a fan-shaped configuration. All five cameras were push-broom scanners, and they all captured the Earth along-track through the same optics, see figure 3.2. It was operational from 1st of may 2002 and until 9th of may 2012, when ESA formally announced the end of all Envisat related missions[3]. It had an impressive signal to noise ratio in the ocean color bands of 1700 to 1, and a spatial resolution of above 1 km to achieve this signal strength. With a nadir swath range of 1150 km, the instrument was able to cover the entire Earth every third day[52].

Furthermore, the MERIS instrument had a downlink of only 15 bands, but they were in return programmable in position, width, and gain, able to adjust the spatial resolution as low as 300 meters. Having an impressive spectral resolution as low as 1.24 nm and a range from 412-1050nm, made the MERIS instrument very versatile [52].

4.2.2 Calibration

A diagram of the MERIS on-board calibration hardware can be found in figure 3.2 [12].

Trending was chosen as a way to update the radiometric calibration coefficient, rather than just updating them frequently upon new observations. This was made possible by monitoring radiometric stability through several approaches e.g. reflectance from deep convective clouds, solar calibration and system vicarious calibration utilizing sites such as MOBY. When it was operational it was often inter-calibrated with MODIS and SeaWiFS, to compare stability and results. The radiometric gain coefficient correction was cross-checked using models for the degradation of optics and diffusers. The diffuser dynamics was closely monitored by having two identical diffusers, but using one a lot less frequently than the other[52].

Spectral stability was monitored through the Erbium-doped diffuser and bi-yearly campaigns correcting wrt. Fraunhofer lines and oxygen A-band measurements[12].

4.3 Sea-viewing Wide Field-of-view Sensor

4.3.1 Mission and instrument

Sea-viewing Wide Field-of-view Sensor, abbreviated SeaWiFS, was a remote sensing instrument designed for ocean color observations[53]. It was the second ocean color remote sensing satellites produced by NASA, building on the experiences from the proof-of-concept Coastal Zone Color Scanner aboard Nimbus-7 [13]. It was operational from 1st of August 1997 to 14th of February 2011 , providing many scientists and oceanographers with valuable data records, and is considered to be one of the most important and influential ocean color sensors to date [1].

The main objective for SeaWiFS was to quantify chlorophyll production of marine phytoplankton, utilizing the 8 bands ranging from 402nm to 885 nm meticulously spread over the spectrum wrt. marine life EMR signatures and atmospheric correction. All bands had a spectral resolution of 20 nm. It was a whiskbroom scanner, and the instrument is depicted in figure 4.2.

4.3.2 Calibration

The pre-launch calibration of SeaWiFS was performed against traceable standards by the National Institute of standards and technology in the USA (NIST). The on-orbit calibration was done by solar calibration using a solar diffuser plaque on a daily basis, and by lunar observations on a monthly basis. thus, providing the instrument with a frequent relative calibration check and a stable long-term absolute calibration check[1].

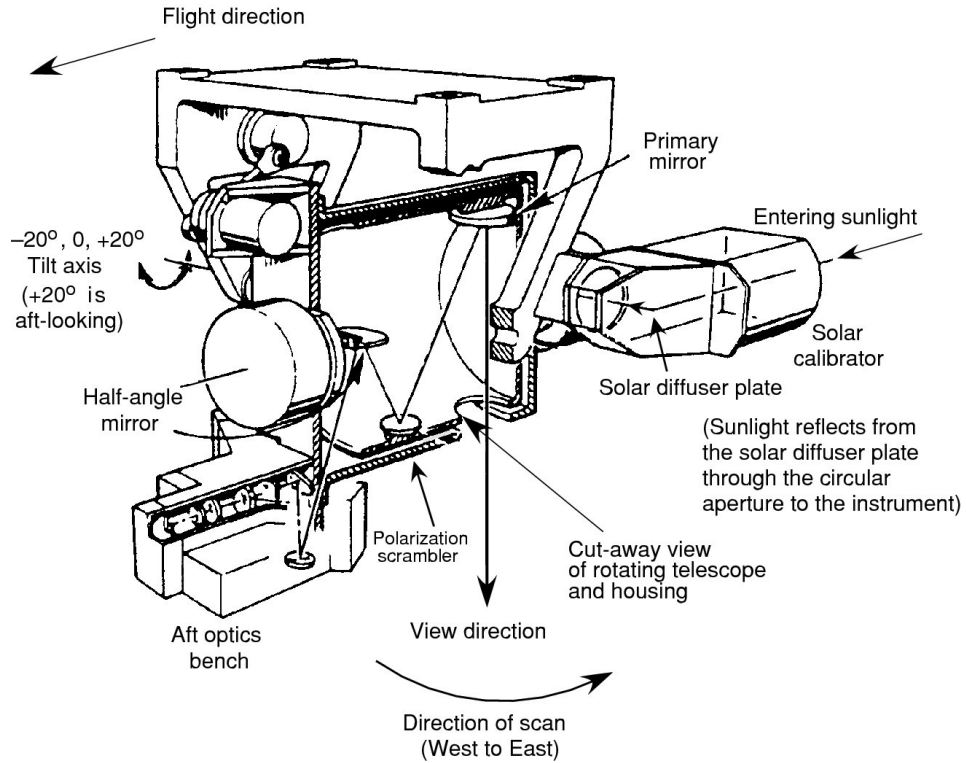


Figure 4.2: A cutaway drawing of the SeaWiFS instrument. Courtesy of S. Martin [1].

Furthermore, the system vicarious calibration was performed using MOBY (see table 3.1), enabling for bias removal of the retrieved water-leaving radiance. As the atmospheric correction of SeaWiFS was highly dependent on the accuracy of the NIR bands, the lunar calibration assured a stable and reliable results[1, 13]., both wrt. data products and vicarious calibration.

With a lifetime in space spanning over 13 years, more than double its life expectancy at launch, the instrument experienced substantial degradation of radiometric sensitivity in all bands. The drift is illustrated in figure 4.3. Despite this degradation, the instrument was still able to provide the ocean color community with valuable data for all its active years. This achievement was accomplished due to the calibration schemes that were applied during operation.

4.3.3 Heritage

The preliminary water-leaving radiance retrieval algorithm designed for SeaWiFS became the basis for most future retrieval algorithms deployed by NASA OBPG and other organizations concerned with ocean color satellites[13, 17, 15, 12].

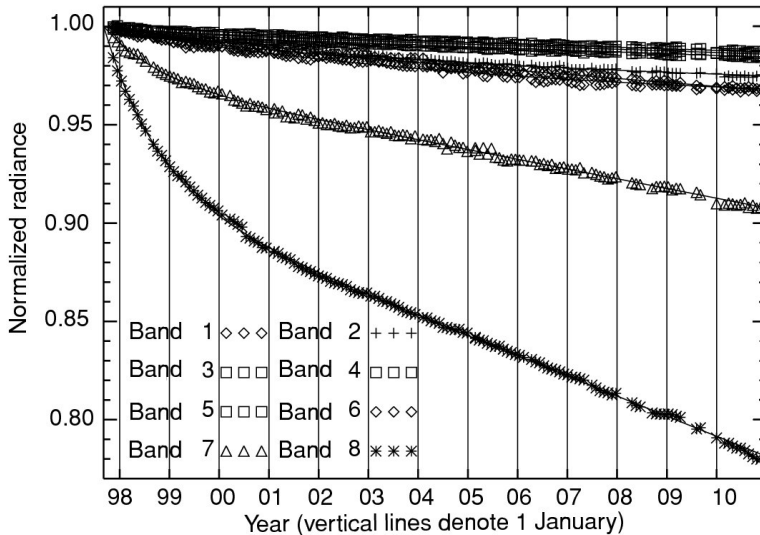


Figure 4.3: The change of sensitivity of in the SeaWiFS instrument, based on Lunar observations and the ROLO model. Image courtesy of S. Martin [1].

4.4 Moderate-resolution Imaging Spectroradiometer

4.4.1 Mission and instrument

Moderate-resolution Imaging Spectrometer, abbreviated MODIS, is a type of instrument with two satellites in orbit currently, Terra and Aqua (often abbreviated MODIST and MODISA respectively)[3]. MODIST was launched 18th of December 1999, and MODISA was launched 4th of May 2002, and both are still monitoring the Earth today. An impressive feat considering that they have a design life of 6 years [54].

The MODIS instruments built to NASA specifications by Santa Barbara Remote Sensing represent the finest in engineering of spaceflight hardware for remote sensing.

It is a sizeable instrument weighing 228.7 kg and consuming on average 162.5 Watts of power[55]. It measures at 36 bands at spatial resolutions ranging from 250 m and up to 1 km, where the ocean color specific bands are 8-16, ranging from 405 nm to 877 nm, with around 20 nm spectral resolution and a spatial resolution of 1 km.

It is designed as a special kind of whiskbroom scanner[1], in the sense that

4.4.2 Calibration

An Illustration photo of the MODIS calibration system can be seen in figure 4.4. Just as with the SeaWiFS, the MODIS instruments uses both lunar and solar observations to monitor radiometric stability and accuracy. In addition to this MODIS uses an interior calibration device called *spectral radiometric calibration assembly* i.e. a device similar

to a monochromator enabling for both spectral and spatial calibration[54]. Thus having 3 sources to perform radiometric calibration from.

Furthermore, a joint calibration between SeaWiFS, MODIST, and MODISA was performed several times in an effort to better characterize their differences and the drift experienced in all sensors. It was in some sense discovered that the measured radiance was highly dependent on viewing angle and there were noticeable differences in the mirror reflectance in both MODIS instruments.

The data from MODIS is radiometrically corrected using look-up-tables rather than trending.

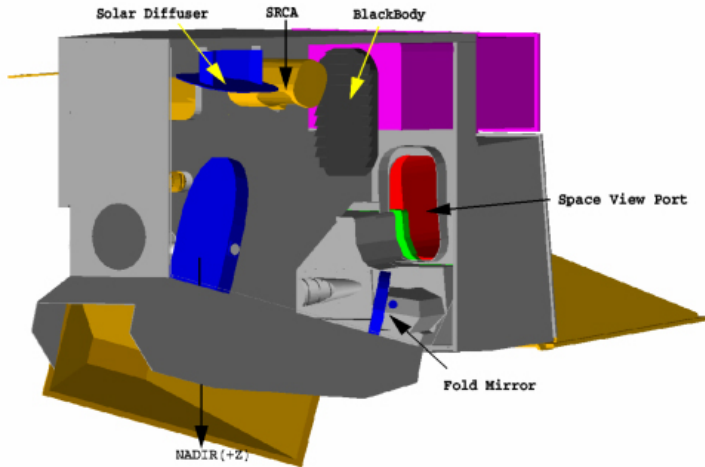


Figure 4.4: An illustration of the MODIS onboard calibration system. Image courtesy of NASA [54].

4.5 The Pre-Aerosol, Clouds and ocean Ecosystem

The Pre-Aerosol, Clouds and ocean Ecosystem mission, abbreviated PACE, is not technically a historical ocean color remote sensing system[3], but it is of particular interest to the NTNU SmallSat Program[5].

Having a scheduled launch in 2022/2023, it is a hyperspectral imager with a planned spectral range from 350 nm to 890 nm at a spectral resolution of 5 nm, and 6 bands in the NIR-SWIR range for atmospheric correction[1]. In some documentation, it is stated that it will have a spatial resolution of 1 km [3], while other sources state that it will be adjustable down to a spatial resolution of 250m [1]. Thus sharing some interesting similarities.

The mission builds on experiences by NASA from MODIS and SeaWiFS i.e. address the shortcomings of prior missions by having bands in the ultraviolet range and a much finer spectral resolution across the entire ocean color relevant range. Further yet it has a lot of useful bands in the NIR-SWIR range for atmospheric correction and classification of atmospheric constituents. When the instrument is operational, data from the mission will be used to develop better atmospheric correction schemes for other hyperspectral instruments.

The tools that are being developed and will be developed for this mission can be of great use to the NTNU SmallSat Program, simply due to the many similarities. The PACE mission will, of course, be a much larger payload, and it will be more refined than a technology demonstration, with clear requirements and expectations. None the less, it is still a relevant mission for all hyperspectral ocean color remote sensing systems[56]. The future of ocean color remote sensing will presumably consist of more hyperspectral instruments[57].

Chapter 5

Simulation

The simulation is based on using modified data from HICO. It is intended as a demonstration of system vicarious calibration. The code provided is not readily implementable to any remote sensing system, due to the nature of the simplistic atmospheric correction approach (see below). This approach was chosen due to the empirical nature of all researched approaches [13, 1, 15, 17], a need for vast datasets with proper *in-situ measurements*, and matching remote sensing observations was moderately difficult to obtain. The concept of vicarious calibration and associated methodology are still presented through the chosen approach.

In the simulations, the sensor is assumed to be well characterized and have ideal sensor behavior i.e.

- The sensor responds only to radiant power in a small band of wavelengths
- The sensor response is not dependent on polarization
- The sensor does not respond to power outside its field of view
- The electrical response and radiant power has a linear relationship

5.1 Methodology and Implementation

A set of case 1 and case 2 water pixels i.e. a pixel near the shore and a pixel far from the shore has been chosen from the original image as shown in figure 5.3. The original pixel spectra retrieved has been treated as the target signal response L_w^t .

As a simple hyperspectral atmospheric correction algorithm for MATLAB has not been made available (see appendix A), Dark Object Subtraction has been used for atmospheric correction[58] i.e. subtracting the spectra from the darkest pixel in all spectra. This simple approach is effective for identifying atmospheric effects in multispectral data, but it should in general not be used for atmospheric correction in hyperspectral data. The pixel with the lowest accumulative RGB value was chosen as the correct atmospheric spectra, and a distortion of this (profile 3 multiplied with 1.1, see figure 5.1b) was applied to generate the wrong/incorrect atmospheric correction.

The degradation dynamics i.e. the reduction in sensitivity, are shown in figure 5.1b. Profile 1 is a tribute to HICO, ad Perpetuam Memoriam, profile 2 is a simple linear degradation model and profile 3 is a bastardization/approximation of the degradation found in figure 4.3, i.e. the degradation experienced at some point during a sensor's lifetime. Profile 0 is no degradation of radiometric sensitivity. This would indicate some quite abrupt changes in radiometric sensitivity. Figure 5.2 is an illustration of how this distortion would affect the captured image in its RGB composition.

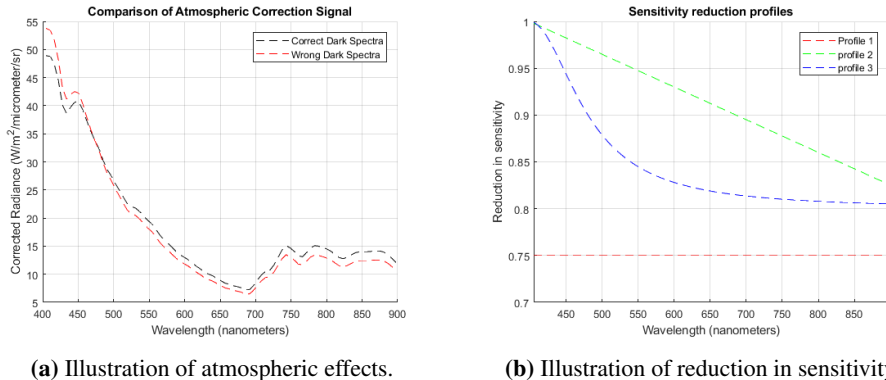


Figure 5.1: Illustration of the degradation performed during the simulations.

Furthermore, noise has been added deterministically i.e. a vector with the number of elements corresponding to the number of wavelengths, with an average of 1 and standard deviation $\sigma = 0.02$ has been element-wisely multiplied with the spectra of the pixel in question.

In addition to this, slight shifts in the spectral dimension have been added to see the effects of spectral shift on the error by moving every spectral response one to the left. The error metrics chosen to analyze the results is the following root mean squared *rmse* expression:

$$rmse = \sqrt{\frac{\sum_{\lambda=1}^n (\hat{L}(\lambda) - L(\lambda))^2}{n}}, \quad n = 87 \quad (5.1)$$

Where $\hat{L}(\lambda)$ is the measured and $L(\lambda)$ is the target. In addition to this the normalized root mean squared was also used as an error metric, calculated in the following way:

$$E_L = \frac{rmse}{\bar{L}}, \quad \bar{L} = \frac{1}{n} \sum_{t=1}^n L(\lambda) \quad (5.2)$$

The different results will be tagged in the bit inspired way depicted in table 5.1. Such that spectra with profile 2 sensitivity degradation, wrong atmospheric correction, noise and no spectral shift would be tagged with the number 2110.

As atmospheric correction is an additive effect, noise and profile are multiplicative effects and a spectral shift is a logical barrel shift operation, the order of operations is not

trivial. The order of operations is described in the *performed action* column of table 5.1, and can be expressed in the following manner as well:

$$distortion = shift(profile(noise(signal))) - atmosphere \quad (5.3)$$

Table 5.1: Table of tags for error dynamics.

Effect	Codes	# performed action
Profile	0, 1, 2, 3	Second
wrong or correct atmospheric correction	1, 0	Fourth
noise added or not	1, 0	First
Spectral shift performed or not	1, 0	Third

5.2 Simulation results

the results are shown in table 5.2.

The selected scene for this simulation can be seen in figure 5.2 and 5.3. The scene was selected due to the fact that it is one of twelve images in the *HICO Sample Image Gallery* [59]. These are scenes of particularly good quality from the HICO mission. The selected image from the gallery is of Noumea in New Caledonia, taken 11th of October 2013 and has scene ID of 14852 in the HICO database.

The effects of distortions are difficult to discover, as can be seen in figure 5.2. In the RGB domain, it is near impossible to directly classify the type of distortion or distortions that have occurred.

let alone see any form of distortion effects, when composed solely form the RGB channels. Thus the value and need for in-depth analysis of retrieved data have been illuminated.

As expected the highest reduction in sensitivity, profile 1, will on average have a higher E_L and $rmse$ value (136.6, 5.64). This corresponds well with the magnitude of the reduced sensitivity, as profile 1 is the largest reduction of sensitivity and it affects each band with the same reduction in sensitivity. Profile 3 is the second most (63.7, 2.65), followed by profile 0 (58.9, 2.41) and Profile 2 (55.88, 2.28). The small difference between profile 3,2 and 0 in E_L and $rmse$ could be due to the fact that the distortion profiles mainly affects the signals with longer wavelengths i.e. signals of low radiance resulting with minimized effect on the error metrics, as the radiance in the shorter wavelengths dominate the error dynamics as a result of their magnitude. Furthermore, this shows that it might be difficult to discover reduced sensitivity based solely on $rmse$ and E_L , and more refined analysis may be needed.

By sorting the results based on $rmse$ or $nrmse$ it becomes clear that the distortion that generates the highest amount of noise, disregarding the effects of the sensitivity reduction, is the added noise. The spectral shift had the second-most effect, and the effects of incorrect atmospheric correction have the least impact on the calculated $rmse$. Given that the uncertainties represented in the incorrect atmospheric correction spectra are of similar character as in the real world, this may support the notion of performing absolute radiometric calibration before performing system calibration. It should be noted that the

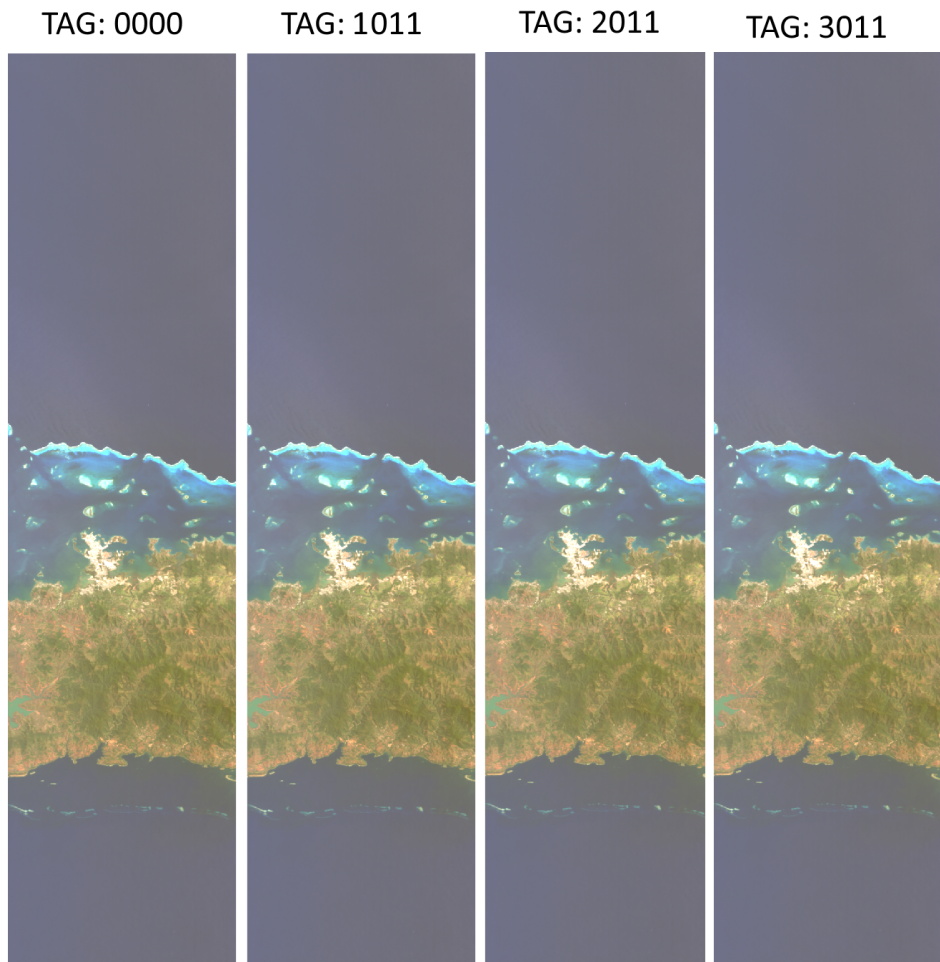


Figure 5.2: An illustration of how the degradation would be perceived in the HICO RGB channels. The TAG is explained in table 5.1. Atmospheric correction is not performed.

reason for performing the operations in this order may also be the fact that you would need accurate TOA radiance to generate correct atmospheric correction in the first place.

The TAG of 0000 seems to have no effect on the pixel, as $E_L = 0$ and $rmse = 0$, which is a welcome result wrt. the validity of the simulation.

A vector for g_i at all wavelengths and \bar{g} was computed for all scenarios but is not provided here.

Furthermore, the software produced to perform this simulation can be used on any .hico.bil file, see appendix B.

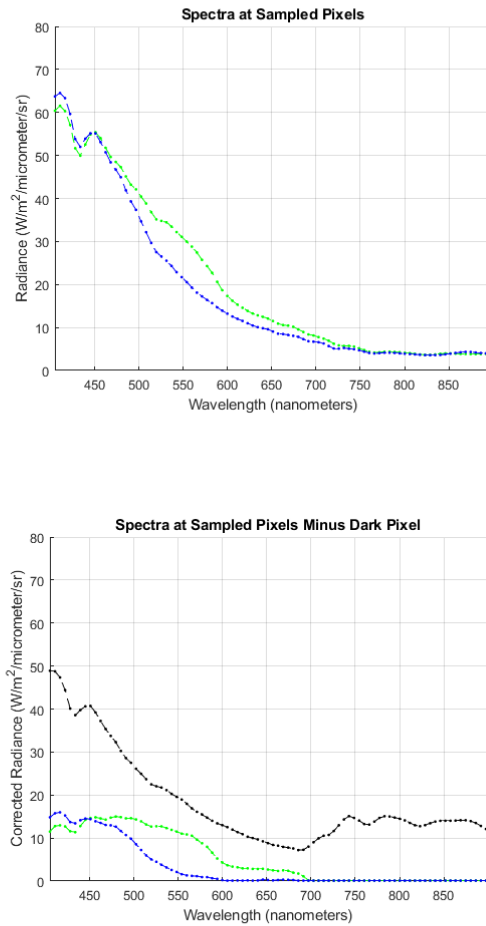


Figure 5.3: An image depicting the selected pixels used for this simulation and their placement in the image. pixel 1 and 2 are green and blue respectively.

Table 5.2: Results from simulations. see figure 5.3 for pixel id.

Pixel	Tag	E_L (%)	$rmse$	Pixel	Tag	E_L (%)	$rmse$
1	0000	0	0.0000	2	0000	0.0000	0.0000
1	0001	31.90	1.7151	2	0001	61.23	2.0276
1	0010	55.67	2.9925	2	0010	87.18	2.8871
1	0011	69.26	3.7232	2	0011	116.30	3.8510
1	0100	24.33	1.3080	2	0100	39.28	1.3007
1	0101	40.67	2.1861	2	0101	71.79	2.3773
1	0110	58.13	3.1245	2	0110	92.98	3.0791
1	0111	73.07	3.9277	2	0111	121.04	4.0081
1	1000	121.35	6.5227	2	1000	181.06	5.9955
1	1001	112.40	6.0415	2	1001	165.24	5.4717
1	1010	107.30	5.7675	2	1010	155.73	5.1569
1	1011	99.54	5.3507	2	1011	146.06	4.8364
1	1100	116.37	6.2549	2	1100	182.47	6.0422
1	1101	108.36	5.8248	2	1101	171.46	5.6777
1	1110	103.88	5.5839	2	1110	163.37	5.4097
1	1111	97.57	5.2445	2	1111	153.00	5.0664
1	2000	17.13	0.9210	2	2000	18.90	0.6261
1	2001	28.30	1.5213	2	2001	54.90	1.8181
1	2010	52.84	2.8405	2	2010	80.82	2.6764
1	2011	63.06	3.3895	2	2011	106.50	3.5268
1	2100	24.33	1.3080	2	2100	39.40	1.3049
1	2101	33.34	1.7922	2	2101	62.29	2.0629
1	2110	52.52	2.8231	2	2110	85.53	2.8322
1	2111	64.75	3.4803	2	2111	109.54	3.6272
1	3000	49.62	2.6676	2	3000	54.94	1.8192
1	3001	44.72	2.4038	2	3001	61.61	2.0402
1	3010	60.31	3.2418	2	3010	80.42	2.6632
1	3011	61.99	3.3322	2	3011	95.55	3.1640
1	3100	47.10	2.5321	2	3100	64.48	2.1354
1	3101	41.12	2.2106	2	3101	63.38	2.0990
1	3110	55.74	2.9963	2	3110	83.83	2.7759
1	3111	59.00	3.1714	2	3111	95.50	3.1626

Discussion & Conclusion

The main finding of this document is that most radiometric calibration approaches regarding remote sensing and ocean color largely have an empirical component, as shown throughout the document and especially in chapter 4. A successful mission, with an objective of performing ocean color observations, often includes a lot of careful analysis of the produced data, possibly over the span of several years. The analysis is important to accurately determine the cause of any eventual discrepancy between what you see and what you expected to see. Through thorough analysis, you would be able to both calibrate and validate the data, still, this process will both need a lot of time and take a lot of time.

Ocean remote sensing literature mainly relies on approaches developed for the multispectral domain, also when performing correction and analysis of hyperspectral data, like data from HICO. The atmospheric correction of HICO images is stated to be unsatisfactory, A. Ibrahim et al. 2018 [17], due to the fact that a couple of bands in the NIR-range is assumed to be *perfect*. They are inherently not *perfect*, and as stated earlier these bands also suffer from low SNR for the HICO platform, i.e. these selected bands are far from *perfect*. However, to be able to compare HICO observations with data from more refined and better-calibrated satellites e.g. MODIS wrt. system performance, it is necessary to perform the same atmospheric correction approach for both systems. The same problem arises when performing analysis on gathered observations to derive ocean color product e.g. estimation of phytoplankton concentration [47]. As technology advances, techniques that before were unattainable or unfitted for certain applications become available. There is a current trend towards equipping remote sensing systems, including the ones made for ocean color observations, with hyperspectral instruments[3]. The NASA PACE mission is an example of this.

As more ocean color satellites with higher spectral resolution, and their subsequent data products, become available better inter-comparison schemes for hyperspectral sensors will become more available as well. Furthermore, techniques used in the fields of chemometrics, food and agriculture analysis[6] that heavily relies on the use of hyperspectral data will become more applicable to ocean color remote sensing. The future of ocean color remote sensing will probably rely more on the hyperspectral domain and associated

methods [57].

The methods discussed in section 3.2 usually needs some kind of extra payload e.g. diffuser plaque. If such an approach is selected for the NTNU SmallSat Program a significant part of the area available will be lost to calibration equipment. However, as has been demonstrated with the HICO mission, it is possible to provide the ocean color community with valuable data, even when such calibration methods are unavailable. Radiometric and system calibration is paramount to provide the scientific community with valuable data, but that is not the same as to say that every available method should be utilized in the calibration of an instrument. Thus, it is important for the NTNU SmallSat Program to find an appropriate subset of calibration approaches for the specific platform. This document suggests an approach similar to that of the HICO mission. The advantage of attitude control, enabling the system to more freely determine what to observe, might be a precious resource for calibration.

6.1 Future work and recommendations

In this section, the next steps, one necessary and one desirable, for the NTNU SmallSat Program is briefly discussed.

6.1.1 Camera characterization

It is important to have a well described, laboratory calibrated, optical sensor before launching any satellite, to have intricate knowledge of the responses of the instrument, to be able to predict degradation and interpret observations in a meaningful way.

A spectral model for the instrument should be developed. There is a need to be familiar with such things as sensitivity wrt. perceived radiance at different wavelengths, polarization sensitivity at different spatial parameters, second-order radiation effects, etc. There is also a need to characterize the camera spatially wrt. the effects of viewing geometry, optical distortion, etc.

Usually, remote sensing instruments going to space are calibrated for a long time before launching. This was not the case for the HICO mission, and even though the instrument was able to produce valuable data throughout its lifetime, there was a great need for calibration and on-orbit fixes. To some extent, one could even claim that the HICO mission was fortunate in many ways, in the sense that a lot of things did not go according to plan, and still the mission was able to produce valuable data for scientist and future ocean color missions. After all, the instrument worked and they were able to discover and relieve most of the complications that arose.

Moreover, even though Spectral calibration was not the main subject of this document, it's still a very important part of ocean color remote sensing. A small shift in wavelengths can, among other things, have an undesirable effect on atmospheric correction. If the atmospheric correction is based on specific bands, these bands need to be sufficiently accurate. To be able to utilize the extra information provided through higher spectral resolution it is necessary to perform spectral calibration as well.

To summarize; there is a great need for proper camera characterization for the NTNU SmallSat Program. This process should start as soon as possible as to not delay launching the satellite.

6.1.2 Hyperspectral Ocean Color Remote Sensing

As stated above, ocean remote sensing has mainly been concerned with multispectral data. The technology to do hyperspectral ocean remote sensing has not been ready [25, 57, 56, 17].

In recent years, however, this technology has become available, and remote sensing satellites are being equipped with hyperspectral sensors. As a result, new algorithms to fully utilize the hyperspectral domain is being developed. This is in its infancy wrt. operational remote sensing, yet it could be useful to follow this development, and to explore different strategies e.g. machine learning and statistical methods, for identifying functional types of phytoplankton[56]. These are methods already being deployed in other approaches to oceanography.

The PACE mission [1, 17] is the first operational hyperspectral ocean remote sensing satellite put forth by NASA OBPG. While developing this system they will also need to develop new algorithms and approaches more suited for the hyperspectral domain. As most of the ocean color literature and successful missions have their origin in NASA, it is safe to assume that following this development will be beneficial for the NTNU SmallSat Program [5].

The future of ocean remote sensing is hyperspectral, and the products of future missions will enable humankind to better understand the oceans that surround us.

Bibliography

- [1] Seelye Martin. *An Introduction to Ocean Remote Sensing*. Cambridge University Press, 2 edition, 2014.
- [2] R. H. Evans and H. R. Gordon. Coastal zone color scanner "system calibration": a retrospective examination. *Journal of Geophysical Research*, 99(C4):7293–7307, 1994.
- [3] Missions & instruments - ioccg. <http://ioccg.org/resources/missions-instruments/>. (Accessed on 12-10-2017).
- [4] Norge som romnasjon / lr om rommet / hjem - norsk romsenter. <https://www.romsenter.no/Lær-om-rommet/Norge-som-romnasjon>. (Accessed on 14-11-2017).
- [5] Mariusz E Grøtte, F Fortuna, Roger Birkeland, Julian Veisdal, Milica Orlandic, Harald Martens, J Tommy Gravdahl, Fred Sigernes, Tor A Johansen, Jan Otto Reberg, Geir Johnsen, and Kanna Rajan. Hyper-spectral imaging Small satellite in multi-agent marine observation system. (Internal Document), 2017.
- [6] Bossoon Park and Renfu Lu. *Hyperspectral imaging Technology in Food and Agriculture*. 2015.
- [7] M. Martens H. Martens. *Multivariate Analysis of Quality: An Introduction*. Wiley, 1 edition, 2000.
- [8] Harald Martens, Tormod Næs, Lennart Eriksson, and Torbjørn Lundstedt. Multivariate calibration. I. Concepts and distinctions. *Trends in Analytical Chemistry*, 3(4):204–210, 2001.
- [9] Ocean optics web book a collaborative web-based book on optical oceanography. <http://www.oceanopticsbook.info/>. (Accessed on 08-09-2017).
- [10] Liguo Wang Chunhui Zhao and Hyperspectral. *Hyperspectral Image Processing*. 2016.

-
- [11] Michael T. Eismann. *Hyperspectral Remote Sensing*. SPIE, 2012.
 - [12] IOCCG. *In-flight Calibration of Satellite Ocean-Colour Sensors*, volume No. 14 of *Reports of the International Ocean Colour Coordinating Group*. IOCCG, Dartmouth, Canada, 2013.
 - [13] Howard R. Gordon and Menghua Wang. Retrieval of water-leaving radiance and aerosol optical thickness over the oceans with SeaWiFS: a preliminary algorithm. *Applied Optics*, 33(3):443, 1994.
 - [14] Ian S. Robinson. The methods of satellite oceanography. *Discovering the Ocean from Space*, pages 7–67, 2010.
 - [15] Bryan A. Franz, Sean W. Bailey, P. Jeremy Werdell, and Charles R. McClain. Sensor-independent approach to the vicarious calibration of satellite ocean color radiometry. *Applied Optics*, 46(22):5068, 2007.
 - [16] IOCCG. *Atmospheric Correction for Remotely-Sensed Ocean-Colour Products*, volume No. 10 of *Reports of the International Ocean Colour Coordinating Group*. IOCCG, Dartmouth, Canada, 2010.
 - [17] Amir Ibrahim, Bryan Franz, Ziauddin Ahmad, Richard Healy, Kirk Knobelgesse, Bo Cai Gao, Chris Proctor, and Peng Wang Zhai. Atmospheric correction for hyperspectral ocean color retrieval with application to the Hyperspectral Imager for the Coastal Ocean (HICO). 2018.
 - [18] M J Montes, B C Gao, and C O Davis. Tafkaa atmospheric correction of hyperspectral data. *Imaging Spectrometry IX*, 5159(January 2004):188–197, 2004.
 - [19] Padmanava Dash, Nan Walker, Deepak Mishra, Eurico D’Sa, and Sherwin Ladner. Atmospheric correction and vicarious calibration of oceansat-1 ocean color monitor (OCM) data in coastal case 2 waters. *Remote Sensing*, 4(6):1716–1740, 2012.
 - [20] Curtiss O Davis and Jasmine Nahorniak. HICO On-Line Atmospheric Correction. 2015.
 - [21] B C Gao, M J Montes, Z Ahmad, and C O Davis. Atmospheric correction algorithm for hyperspectral remote sensing of ocean color from space. *Applied optics*, 39(6):887–896, 2000.
 - [22] IOCCG. *IOCCG Report Number 07: Why ocean colour? The societal benefits of ocean-colour technology*. Number 7. 2008.
 - [23] S Bagheri. *Hyperspectral Remote Sensing of Water Quality*. 2017.
 - [24] Howard R Gordon, Otis B Brown, and Michael M Jacobs. Computed Relationships Between the Inherent and Apparent Optical Properties of a Flat Homogeneous Ocean.
-

-
- [25] IOCCG. *Minimum Requirements for an Operational Ocean-Colour Sensor for the Open Ocean*, volume No. 1 of *Reports of the International Ocean Colour Coordinating Group*. IOCCG, Dartmouth, Canada, 1998.
- [26] Henry B. Garrett. *Space Environments and Survivability*, pages 37–59. Springer Berlin Heidelberg, Berlin, Heidelberg, 2014.
- [27] Ceos. <http://ceos.org/>. (Accessed on 08-11-2017).
- [28] Objectives and terms of reference - ioccg. <http://ioccg.org/about/objectives-and-terms-of-reference/>. (Accessed on 08-12-2017).
- [29] Gyanesh Chander, Tim J. Hewison, Nigel Fox, Xiangqian Wu, Xiaoxiong Xiong, and William J. Blackwell. Overview of intercalibration of satellite instruments. *IEEE Transactions on Geoscience and Remote Sensing*, 51(3):1056–1080, 2013.
- [30] Bo-Cai Gao, Rong-Rong Li, Robert L. Lucke, Curtiss O. Davis, Richard M. Bevilacqua, Daniel R. Korwan, Marcos J. Montes, Jeffrey H. Bowles, and Michael R. Corson. Vicarious calibrations of HICO data acquired from the International Space Station. *Applied Optics*, 51(14):2559, 2012.
- [31] Robert L. Lucke, Michael Corson, Norman R. McGlothlin, Steve D. Butcher, Daniel L. Wood, Daniel R. Korwan, Rong R. Li, Willliam A. Snyder, Curt O. Davis, and Davidson T. Chen. Hyperspectral Imager for the Coastal Ocean: instrument description and first images. *Applied Optics*, 50(11):1501, 2011.
- [32] Hugh H. Kieffer and Thomas C. Stone. The Spectral Irradiance of the Moon. *The Astronomical Journal*, 129(6):2887–2901, 2005.
- [33] Stphane Colzy, Aim Meygret, Gwendoline Blanchet, and Lydwine Gross-Colzy. Improving ROLO lunar albedo model using PLEIADES-HR satellites extra-terrestrial observations. *Earth Observing Systems XXII*, (September):82, 2017.
- [34] Shuo Ma, Wei Yan, Yun-Xian Huang, Wei-Hua Ai, and Xianbin Zhao. Vicarious calibration of S-NPP/VIIRS daynight band using deep convective clouds. *Remote Sensing of Environment*, 158:42–55, 2015.
- [35] Philip N. Slater, Stuart F. Biggar, James M. Palmer, and Kurtis J. Thome. *Unified approach to pre- and in-flight satellite-sensor absolute radiometric calibration*, volume 2583, pages 130–141. 1995.
- [36] Space-grade spectralon diffuse reflectance material - labsphere — internationally recognized photonics company. <http://www.labsphere.com/labsphere-products-solutions/materials-coatings-2/coatings-materials/space-grade-spectralon-diffuse-reflectance-material/>. (Accessed on 09-12-2017).
- [37] Joel McCorkel, Kurtis Thome, and Lawrence Ong. Vicarious calibration of eo-1 hyperion. *IEEE Journal of Selected Topics in Applied Earth Observations and Remote Sensing*, 6(2):400–407, 2013.

-
- [38] Nasa ocean color. <https://oceancolor.gsfc.nasa.gov/>. (Accessed on 10-10-2017).
 - [39] David R. Doelling, Daniel Morstad, Benjamin R. Scarino, Rajendra Bhatt, and Arun Gopalan. The characterization of deep convective clouds as an invariant calibration target and as a visible calibration technique. *IEEE Transactions on Geoscience and Remote Sensing*, 51(3):1147–1159, 2013.
 - [40] Steve Graham. Clouds & Radiation Fact Sheet Feature Articles. *NASA Earth Observatory*, pages 1–6, 3 1999.
 - [41] Rajendra Bhatt, David R. Doelling, Benjamin Scarino, Conor Haney, and Arun Gopalan. Development of seasonal BRDF models to extend the use of deep convective clouds as invariant targets for satellite SWIR-band calibration. *Remote Sensing*, 9(10):1061, 2017.
 - [42] Patrice; Morel André; Antoire David; Montagner Franois Fougnie, Bertrand; Henry. Identification and characterization of stable homogeneous oceanic zones: Climatology and impact on in-flight calibration of space sensors over Rayleigh scattering. (1), 1999.
 - [43] Charles Cox and Walter Munk. Measurement of the roughness of the sea surface from photographs of the sun’s glitter. *J. Opt. Soc. Am.*, 44(11):838–850, Nov 1954.
 - [44] Giuseppe Zibordi and Frdric Mélin. An evaluation of marine regions relevant for ocean color system vicarious calibration. *Remote Sensing of Environment*, 190:122–136, 2017.
 - [45] Robert E. Carlson. A trophic state index for lakes1. *Limnology and Oceanography*, 22(2):361–369, 1977.
 - [46] Dennis K. Clark, Mark a. Yarbrough, Mike Feinholz, Stephanie Flora, William Broenkow, Yong Sung Kim, B. Carol Johnson, Steven W. Brown, Marilyn Yuen, and James L. Mueller. MOBY, A Radiometric Buoy for Performance Monitoring and Vicarious Calibration of Satellite Ocean Color Sensors: Measurement and Data Analysis Protocols. VI(May 2014):3–34, 2003.
 - [47] Wesley J. Moses, Anatoly A. Gitelson, Sergey Berdnikov, Jeffrey H. Bowles, Vasiliy Povazhnyi, Vladislav Saprygin, Ellen J. Wagner, and Karen W. Patterson. HICO-based NIR-red models for estimating chlorophyll-a concentration in productive coastal waters. *IEEE Geoscience and Remote Sensing Letters*, 11(6):1111–1115, 2014.
 - [48] D. R. Korwan, R. L. Lucke, N. R. McGlothlin, S. D. Butcher, D. L. Wood, J. H. Bowles, M. Corson, W. A. Snyder, C. O. Davis, and D. T. Chen. Laboratory characterization of the Hyperspectral Imager for the Coastal Ocean (HICO). *International Geoscience and Remote Sensing Symposium (IGARSS)*, 2:69–72, 2009.
 - [49] Nasa pace - home. <https://pace.gsfc.nasa.gov/>. (Accessed on 11-12-2017).
-

-
- [50] M. D. Lewis, R. W. Gould, R. A. Arnone, P. E. Lyon, P. M. Martinolich, R. Vaughan, A. Lawson, T. Scardino, W. Hou, W. Snyder, R. Lucke, M. Corson, M. Montes, and C. Davis. The Hyperspectral Imager for the Coastal Ocean (HICO): Sensor and data processing overview. *OCEANS 2009, MTS/IEEE Biloxi - Marine Technology for Our Future: Global and Local Challenges*, pages 1–9, 2009.
- [51] Meris - ioccg. <http://ioccg.org/sensor/meris/>. (Accessed on 11-12-2017).
- [52] Meris instrument calibration. https://earth.esa.int/c/document_library/get_file?uuid=ccaeefb98-d7f0-4117-b1ea-c30a25a9821d&groupId=10174. (Accessed on 12-12-2017).
- [53] Seawifs - ioccg. <http://ioccg.org/sensor/seawifs/>. (Accessed on 11-12-2017).
- [54] Modis web. <https://modis.gsfc.nasa.gov/about/components.php>. (Accessed on 12-12-2017).
- [55] Modis - aqua - ioccg. <http://ioccg.org/sensor/modis-aqua/>. (Accessed on 11-12-2017).
- [56] IOCCG. *Phytoplankton Functional Types from Space*, volume No. 15 of *Reports of the International Ocean Colour Coordinating Group*. IOCCG, Dartmouth, Canada, 2014.
- [57] IOCCG. *Mission Requirements for Future Ocean-Colour Sensors*, volume No. 13 of *Reports of the International Ocean Colour Coordinating Group*. IOCCG, Dartmouth, Canada, 2012.
- [58] 'dark-object-subtraction' tag wiki - geographic information systems stack exchange. <https://gis.stackexchange.com/tags/dark-object-subtraction/info>. (Accessed on 13-12-2017).
- [59] Hico - sample image gallery. <http://hico.coas.oregonstate.edu/gallery/gallery-scenes.php>. (Accessed on 16-12-2017).

Appendices

Appendix

A

Correspondence

In this section, the correspondence I was able to get with persons of significance within the remote sensing community is provided. Q is denoted as my voice, A is denoted as the voice of the recipient.

Table A.1: Correspondence with Thomas C. Stone at US Geological Survey in Flagstaff.

Speaker	Answer	Date
Q	<p>Hi!</p> <p>My background is control theory and electrical engineering, but as a part of a project, I am trying to learn more about how to do an on-orbit calibration of earth observing satellites.</p> <p>Your name was mentioned as here as the person to contact regarding modeling of the moons irradiance (and perhaps even radiance?) If you could help me figure out how to, in a good way, simulate how the moon will behave given certain outputs that would be very helpful and much appreciated.</p> <p>Again, any help is appreciated.</p>	8 th of November 2017, 12.53
A	<p>Hello Sivert Bakken - thanks for contacting me regarding lunar calibration. Yes, on-orbit calibration of Earth-observing satellite instruments is what I do. I'm not sure how much I can help you, but I would be happy to chat a bit on the phone with you if you want to call.</p> <p>A good reference for background is: "The Spectral Irradiance of the Moon," Astronomical Journal 129, pp. 2887-2901 (2005)</p> <p>Best regards, Tom Stone</p>	9 th of November 2017, 02.12
Q	<p>Great to know that I have come to the right person!</p> <p>Due to the time zones, I believe that chatting on the phone will be somewhat impractical, unfortunately.</p> <p>What I want to do is to simulate the reflectance in MATLAB. It probably already exists something that does this, but I have not been able to find it. Is the model described here: Link to Website the one most up to date, or are there any other forms models more accurate. I have found some papers claiming that they get more persistent results when comparing data from several satellites in the visual-NIR bands.</p>	9 th of November 2017, 10.16

This seemed promising after the initial answer, but I never got a 2nd answer.

Table A.2: Correspondence with Bryan A. Franz. Bryan Franz is a Research Scientist and Assistant Chief for Science Research in the Ocean Ecology Laboratory at NASA Goddard Space Flight Center. Click here to see bio.

Speaker	Answer	Date
Q	<p>I am a student at NTNU researching ocean remote sensing in an attempt to better understand how a multi-agent marine observation system utilizing UAVs and ASVs could be used in combination with observations obtained through satellite.</p> <p>Thus I am particularly interested in the HICO case, as it has many factors similar to the system that I am working on.</p> <p>I was hoping that you could help me since your name shows up everywhere :)</p> <p>Currently, I am trying to do the atmospheric correction for the hyperspectral case, but I have not been able to find any readily deployable code for MATLAB. As I just want something to just familiarize with the physical behavior I was wondering if you know of anything I could use.</p> <p>I recently came across this paper[17] and this code, but I am not sure how to use any of this information.</p> <p>Is there any sort of atmospheric correction for hyperspectral data made for MATLAB anywhere?</p>	17 th of November 2017, 08.56
A	<p>Sivert,</p> <p>I dont use matlab, and in practice an interpreted language is not efficient enough for satellite data processing.</p> <p>The code you were looking at is distributed with user interface through Seadas. It will transform the HICO data into the multispectral domain before performing atmospheric correction.</p>	17 th of November 2017, 12.32

Table A.3: Correspondence with Jasmine Nahorniak, HICO Project Scientist

Speaker	Answer	Date
Q	<p>Hi!</p> <p>I am a student at NTNU researching ocean remote sensing in an attempt to better understand how a multi-agent marine observation system utilizing UAVs and ASVs could be used in combination with observations obtained through satellite. Thus I am particularly interested in the HICO case, as it has many factors similar to the system that I am working on.</p> <p>Following this thread, I was led to believe that it was trivial to get the spectra of the HICO data without atmospheric effects, but I am not able to get the web app to work. Do you have anything software that may help me process one of the gallery scenes, preferably in MATLAB?</p> <p>Any information is appreciated! :)</p>	18 th of November 2017, 12.32
A	<p>Sivert,</p> <p>Unfortunately the server that hosted the online HICO atmospheric correction software is no longer functional. However, NASA provides free software (SeaDAS) that you can use to process HICO data (as well as data from many other ocean color satellites).</p> <p>Regards, Jasmine.</p>	20 th of November 2017, 10.39

Table A.4: Correspondence with Curt Davis, HICO Project Scientist.

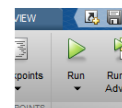
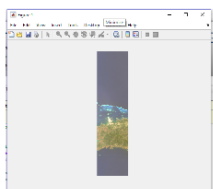
Speaker	Answer	Date
Q	<p>Hi!</p> <p>I am a student at NTNU researching ocean remote sensing in an attempt to better understand how a multi-agent marine observation system utilizing UAVs and ASVs could be used in combination with observations obtained through satellite. Thus I am particularly interested in the HICO case, as it has many factors similar to the system that I am working on.</p> <p>Following this thread, I was led to believe that it was trivial to get the spectra of the HICO data without atmospheric effects, but I am not able to get the web app to work. Do you have anything software that may help me process one of the gallery scenes, preferably in MATLAB?</p> <p>Any information is appreciated! :)</p>	18 th of November 2017, 12.32
A	<p>Sivert, The OSU HICO site is no longer supported and our atmospheric correction tool no longer works. Go to the NASA Ocean Color Site to get the data and they do some atmospheric correction which works for most images.</p> <p>http://oceancolor.gsfc.nasa.gov/</p> <p>Cheers! Curt Davis</p>	20 th of November 2017, 18.23

Appendix B

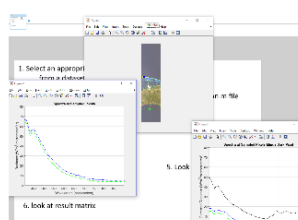
How to perform simulation

The simulation should be straightforward to perform. Given that you have found a .hico.bil file that you want to investigate, you'll only need to run the simulation.m file from your MATLAB window. A file explorer window will then pop-up and you'll have to select the desired .hico.bil file to investigate. After selecting the file, the image will be loaded into your MATLAB workspace and you'll be asked to select two pixels in this image to investigate. The spectra from the two pixels you selected will be plotted, with and without dark pixel atmospheric correction. At this point, there will also be two tables containing all of the variables discussed in this document named results p1 and results p2. See below for a more visual step-by-step guide.

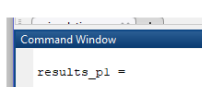
1. Select an appropriate .hico.bil file from a dataset provider



2. Run the simulation.m file



3. Select pixels to investigate



4. Look at plots



5. look at result matrix